Enclosure 2

KP-FHR Fuel Performance Methodology Topical Report, Revision 3

(Non-Proprietary)

Kairos Power LLC
707 W. Tower Ave
Alameda, CA 94501

KP-FHR Fuel Performance Methodology

Topical Report

Revision No. 3
Document Date: June 2021

Non-Proprietary

COPYRIGHT Notice

Rev	Description of Change	Date
0	Initial Issuance	December 2019
1	Update of Validation and Uncertainty Sections	March 2020
2	Update of Uncertainty and Methodology Sections	November 2020
3	Update Uncertainty Section	June 2021

Executive Summary

This report describes the methodology and analytical codes used to conduct fuel performance analysis of uranium oxycarbide (UCO) tristructural isotropic (TRISO)-coated particle fuel for the Kairos Power Fluoride Salt-Cooled High-Temperature Reactor (KP-FHR).

The layers of TRISO-coated fuel particles are engineered to provide retention of fission products and provide a "functional containment." Analytical models have been developed to model TRISO-coated fuel particles and assess their structural integrity and leak-tightness with respect to the potential release of fission products from the fuel particle layers. The fuel performance code BISON, developed and maintained at Idaho National Laboratory (INL), provides a basis for performing these types of analyses. Modifications have been made to the INL-developed code to reflect KP-FHR design specific fuel form and the updated code is referred to as KP-BISON.

This report describes the KP-FHR fuel behavior, modeling of physical properties, as well as the methodology used to develop a UCO TRISO model in KP-BISON. This model will be used to predict the performance behavior of TRISO fuel under KP-FHR normal operating conditions, anticipated operational occurrences, design-basis events, and beyond-design-basis events using constitutive equations and analytical relationships developed from experimental data.

This report also describes the verification and validation of KP-BISON for use in performing safety and licensing basis fuel performance analysis of the KP-FHR. The verification and validation of the KP-BISON code assesses the uncertainties in the analysis and methodology for modeling the fuel. KP-FHR example analyses are also provided.

Table of Contents

Acronyms

AGR	Advanced Gas Reactor
BAF	Bacon Anisotropy Factor (degree of anisotropy)
CFR	Code of Federal Regulations
CRP	Coordinated Research Program
C/U	Carbon to Uranium Ratio
DOE	Department of Energy
FHR	Fluoride Salt-Cooled High Temperature Reactor
FIMA	Fissions per Initial (heavy) Metal Atom
FOM	Figure Of Merit
HALEU	High-Assay Low-Enriched Uranium
HFR	High Flux Reactor
HTGR	High Temperature Gas-cooled Reactor
IAEA	International Atomic Energy Agency
INL	Idaho National Laboratory
IPyC	Inner Pyrolytic Carbon
KP	Kairos Power
KP-FHR	Kairos Power Fluoride Salt-Cooled High Temperature Reactor
LWR	Light Water Reactor
MC	Monte Carlo
MHTGR	Modular High Temperature Gas-Cooled Reactor
MOOSE	Multiphysics Object-Oriented Simulation Environment
M&S	Modeling and Simulation
NRC	Nuclear Regulatory Commission
OPyC	Outer Pyrolytic Carbon
O/U	Oxygen to Uranium Ratio
PARFUME	Particle Fuel Model (INL TRISO fuel performance code)
PDC	Principal Design Criteria
PIE	Post-Irradiation Examination
PIRT	Phenomena Identification and Ranking Table
PyC	Pyrolytic Carbon (Pyrocarbon)
R/B	Release Rate to Birth Rate Ratio
RF	Release Fraction
RG	Regulatory Guide
SARRDL	Specified Acceptable System Radionuclide Release Design Limits
SiC	Silicon Carbide
TRISO	Tristructural Isotropic
UCO	Uranium Oxycarbide (a mixture of UC, UC_2, and UO_2)
U.S.	United States
UQ	Uncertainty Quantification
V&V	Verification and Validation

1   INTRODUCTION

Kairos Power LLC (Kairos Power) is pursuing the design, licensing, and deployment of the Kairos Power Fluoride Salt-Cooled High Temperature Reactor (KP-FHR). To support these objectives, Kairos Power has developed a fuel performance methodology to perform the fuel design and analysis of the KP-FHR tristructural isotropic (TRISO)-coated particle fuel. The objective of this methodology is to assess the structural integrity and leak-tightness to the release of fission products from the KP-FHR fuel.

The fuel performance methodology described in this report is comprised of two main elements, the methodology for modeling and performing the fuel performance analyses, and the description of the analytical computer code (KP-BISON) which implements the methodology. The fuel performance methodology includes a consideration of fuel performance uncertainties. The description of the finite element code includes the modifications made to the underlying BISON code, developed by Idaho National Laboratory (INL), to accommodate the KP-FHR fuel design, including code verification and validation. The modified code is called KP-BISON. Examples of fuel performance analysis are also provided as a demonstration of the implementation of the fuel performance methodology. Implementation of the methodology and the results of fuel performance analyses will be provided as part of license applications submitted under the Code of Federal Regulations (CFR), 10 CFR 50 or 10 CFR 52.

The methodologies provided in this report are applicable to fuel performance analyses for normal operating conditions, anticipated operational occurrences, design-basis events, and beyond design basis events.

The initial section provides a description of the high-level design features that represent the fundamental technologies of the KP-FHR and establish a basis of applicability for the fuel performance methodologies. The initial section also discusses the relevant regulatory requirements that support the requested safety evaluation findings. Section 2 provides a description of TRISO fuel behavior and identifies the significant failure modes that are modeled in KP-BISON. Section 3 addresses the material properties and physical models that are used in the fuel performance analysis methodology. Section 4 describes the verification and validation of the KP-BISON code and also describes the supporting sensitivity analyses that are performed to assess analysis methodology and to establish code uncertainties. Section 5 describes the KP-BISON code and the changes being made to the underlying BISON code. Section 6 provides the methodology for performing a fuel performance analysis, and the limitations on the use of KP-BISON. Example results from KP-BISON calculations are provided in Appendix C.

Fuel performance is defined as the ability of nuclear fuel to sustain neutron irradiation while keeping its physical integrity. For TRISO fuel, it is measured by assessing the probability of failure of the coating layers and the potential release of fission products. Because of the probabilistic nature of fuel failure (Sections 3.1.3.7 and 3.1.5.5), the assessment includes a statistical treatment of a population of TRISO particles.

1.1   DESIGN FEATURES

1.1.1   Design Background

To facilitate Nuclear Regulatory Commission (NRC) review and approval of this report for use by future applicants, key design features are provided in Section 1.1.2 which are inherent to the KP-FHR technology. These features are not expected to change during the design development by Kairos Power and provide the basis to support the safety evaluation of this report. Should fundamental changes occur to these key design features, or new or revised regulations be promulgated that affect the methodology

and conclusion in this report, such changes would be reconciled and addressed in license application submittals.

The KP-FHR is a U.S.-developed Generation IV advanced reactor technology. In the last decade, U.S. national laboratories and universities have developed pre-conceptual Fluoride High-Temperature Reactor (FHR) designs with different fuel geometries, core configurations, heat transport system configurations, power cycles, and power levels. More recently, University of California at Berkeley developed the Mark 1 pebble-bed FHR, incorporating lessons learned from the previous decade of FHR pre-conceptual designs. Kairos Power has built on the foundation laid by Department of Energy (DOE)-sponsored university Integrated Research Projects (IRPs) to develop the KP-FHR.

Although not intended to support the findings necessary to approve this topical report, additional design description information is provided in the technical report "Design Overview of the Kairos Power Fluoride Salt-Cooled, High Temperature Reactor" (Reference 1).

1.1.2   Key Design Features of the KP-FHR

The KP-FHR is a high temperature reactor with molten fluoride salt coolant operating at near-atmospheric pressure. The fuel in the KP-FHR is based on the TRISO high-temperature, carbonaceous-matrix coated particle fuel (originally developed for High Temperature Gas-cooled Reactors - HTGRs) in a pebble fuel element. Coatings on the particle fuel provide retention of fission products. The reactor coolant is a chemically stable molten fluoride salt mixture, $2\times^7$LiF:BeF$_2$ (Flibe) which also provides retention of fission products that escape from any fuel defects. A primary coolant loop circulates the reactor coolant using pumps and transfers the heat to an intermediate coolant loop via a heat exchanger. The pumped flow intermediate coolant loop utilizes a nitrate salt, compatible with the reactor coolant, and transfers heat from the reactor coolant to the power conversion system through a steam generator. The design includes two decay heat removal systems. The design includes decay heat removal for both normal conditions and accident conditions. The design also includes a passive decay heat removal function, which along with natural circulation in the reactor vessel, is used to remove decay heat in response to a design basis accident. The KP-FHR does not rely on electrical power to achieve and maintain safe shutdown for design basis accidents.

The KP-FHR design relies on a functional containment approach similar to the Modular High Temperature Gas-Cooled Reactor (MHTGR) instead of the typical light water reactor (LWR) low-leakage, pressure retaining containment structure. The KP-FHR functional containment safety design objective is to meet 10 CFR 50.34 (10 CFR 52.79) offsite dose requirements at the plant's exclusion area boundary with margin. A functional containment is defined in Regulatory Guide (RG) 1.232, "Guidance for Developing Principal Design Criteria for Non-Light water Reactors" as a "barrier, or set of barriers taken together, that effectively limit the physical transport and release of radionuclides to the environment across a full range of normal operating conditions, anticipated operational occurrences, and accident conditions." As also stated in RG 1.232, the NRC has reviewed the functional containment concept and found it "generally acceptable," provided that "appropriate performance requirements and criteria" are developed. The NRC staff has developed a proposed methodology for establishing functional containment performance criteria for non-LWRs, which is presented in SECY-18-0096, "Functional Containment Performance Criteria for Non-Light-Water-Reactors". This SECY document has been approved by the Commission.

The functional containment approach for the KP-FHR is to control radionuclides primarily at their source within the coated fuel particle under normal operations and accident conditions without

requiring active design features or operator actions. The KP-FHR design relies primarily on the multiple barriers within the TRISO fuel particles and fuel pebble to ensure that the dose at the site boundary as a consequence of postulated accidents meets regulatory limits. However, in contrast to the MHTGR, the KP-FHR molten salt coolant also serves as an additional distinct barrier providing retention of fission products that escape the fuel particle and fuel pebble barriers. This additional retention barrier is a key feature of the enhanced safety and reduced source term in the KP-FHR.

1.2   REGULATORY REVIEW

The PDC for the KP-FHR have been established in the Kairos Power Topical Report, "Principal Design Criteria for the Kairos Power Fluoride Salt-Cooled High Temperature Reactor" (Reference 2). The specific PDC in this report relevant to fuel performance and functional containment aspects of the TRISO fuel particle of the KP-FHR are PDC 10 and PDC 16. These PDC are discussed below.

Fuel performance is relevant to demonstrating conformance to PDC 10 because the reactor fuel design functions to control the release of fission products within limits. PDC 10 states:

> *The reactor system and associated heat removal, control, and protection systems shall be designed with appropriate margin to ensure that specified acceptable system radionuclide release design limits are not exceeded during any condition of normal operation, including the effects of anticipated operational occurrences.*

Fuel performance is also relevant to demonstrating conformance to PDC 16 because the design of the KP-FHR TRISO fuel contains four fission product barriers, which along with the molten salt coolant constitute the functional containment for the KP-FHR. PDC 16 states:

> *A reactor functional containment, consisting of multiple barriers internal and/or external to the reactor and its cooling system, shall be provided to control the release of radioactivity to the environment and to ensure that the functional containment design conditions which are safety significant are not exceeded for as long as postulated accident conditions require.*

Both PDC 10 and PDC 16 relate to ensuring that the specified acceptable system radionuclide release design limits (SARRDLs) are not exceeded. The fuel performance analysis methodology described in this topical report is used to predict the integrity of the fuel and its capability to retain fission products which directly impacts the SARRDLs. The methodology in this report defines the set of fuel design limits that ensure the SARRDLs are not exceeded. These limits are implemented in the design and qualification of the KP-FHR fuel which is addressed in a separate topical report.

The other fuel related regulations are those in 10 CFR 50.34, "Contents of Applications: Technical Information" and 10 CR 50.46, "Acceptance Criteria for emergency core cooling systems for light-water nuclear power plants." The pertinent regulations in 10 CFR 50.34 relate to the analysis of the design and performance of structures, systems, and components with the objective of assessing the risk to the public health resulting from operation of the facility. In addition, 10 CFR 50.34 requires the determination of margins of safety during normal operation and transients that are anticipated during the life of the facility. The regulations in 10 CFR 50.46 are discussed in the "Regulatory Analysis for the Kairos Power Fluoride Salt-Cooled High Temperature Reactor," and are determined to be not applicable to non-LWRs such as the KP-FHR.

In addition to 10 CFR 50.34 and 10 CFR 50.46, 10 CFR 100 relates to the acceptability of a reactor site and fission product release to the environment following a major accident scenario is applicable because the fuel contains the primary barriers to the release of radioactivity. The fuel performance analysis determines the number of fuel failures which directly supports the radiological analysis.

Kairos Power requests that the NRC review and approve the fuel performance analysis methodology in Section 6, the fuel performance uncertainty quantification methodology, and acceptability of the KP-BISON computer code as described in this topical report to be used for conducting fuel performance analysis for a KP-FHR which demonstrate conformance to the cited regulations. This methodology applies to fuel performance for a non-power or power KP-FHR as defined in 10 CFR 50.2.

2 FUEL BEHAVIOR

2.1 FUEL DESCRIPTION

The KP-FHR fuel design consists of TRISO-coated particles embedded in an annular shell inside a spherical pebble to form a fuel element (Figures 2-1 and 2-2). The pebble contains a central sub-dense inner core surrounded by an annular layer of TRISO particles packed into partially-graphitized matrix material (fuel annulus) and covered by an outer shell of fuel-free matrix material. Each TRISO particle is composed of a fissile uranium oxycarbide (UCO) kernel surrounded by successive coating layers consisting of a porous carbon buffer layer, a dense inner pyrolytic carbon (IPyC) layer, a silicon carbon (SiC) layer, and a dense outer pyrolytic carbon (OPyC) layer. The TRISO particles are overcoated with resinated graphite powder before being pressed into the fuel annulus. The resinated graphite powder transforms into "so-called" matrix material upon pressing and subsequent heat treatments. The KP-FHR fuel kernel uses UCO instead of UO_2 because it less likely to produce carbon monoxide (CO) as discussed later in this report.

The primary functions of the fuel components are described in Table 2-1. Typical KP-FHR fuel properties are provided in Table 2-2. Dispersed uranium contamination and coating layer defect levels are in Table 2-3. Note that the content in these tables is provided for information only and to facilitate review and approval of the analytical methodologies, models, and analytical codes. The KP-FHR fuel specifications are expected to be very similar. Review and approval of the KP-FHR fuel design will be requested as part of a separate topical report on fuel qualification. The content in these tables corresponds to the fuel specifications of the Advanced Gas Reactor (AGR)-5/6/7 irradiation test (Reference 5). This test was the fourth irradiation campaign of the DOE AGR Fuel Development and Qualification Program and served as a fuel qualification and margin test. Table 2-5 provides a high-level summary of the AGR testing programs that are referred to in this document.

In Table 2-3, dispersed uranium is defined as uranium that is present outside of a fission gas retentive layer, primarily as contamination on or within the OPyC layer or as dispersed within the partially graphitized matrix material, from the fuel particle manufacturing process. Exposed kernels are TRISO particles that have sustained mechanical damage after coating and have substantially cracked or broken coating layers. Dispersed uranium and exposed kernels combine to form the more generic heavy metal contamination. Additionally, some particles can sustain damage in only one of their coating layers (PyC or SiC) and this is quantified using specific defect fractions. Heavy metal contamination and defective layers both contribute to the release of fission products from the fuel element and are an important aspect of fuel fabrication and fuel performance. Finally, Table 2-4 provides representative values for the properties of the KP-FHR pebble.

2.2 FUEL PERFORMANCE

2.2.1 TRISO Fuel Behavior During Normal Operation, AOOs, and Design Basis Accidents

The primary function of the three outer coating layers (IPyC, SiC, and OPyC) of a TRISO particle is to contain fission products produced in the kernel (key part of the functional containment). The loss of structural integrity and leak-tightness to fission products of a coating layer constitutes a failure of this coating layer. Coating failures are categorized as either a "TRISO failure" or "SiC failure". TRISO failure,

also referred to as an "exposed kernel", corresponds to the loss of integrity of all three outer coating layers and is detected by the release of fission gases. Conversely, SiC failure corresponds to the loss of integrity of the SiC layer, the primary barrier to the release of fission products, with at least one remaining intact PyC layer such that fission gases are retained in the TRISO particle. SiC failure is usually detected by the release of cesium. These failures can occur when TRISO-coated fuel particles undergo neutron irradiation. For KP-FHR, the expected normal operating conditions of the fuel in the startup, transition, and equilibrium cores are provided in Table 2-6. The maximum SiC and kernel temperatures shown in Table 2-6 will be determined by the temperature of the surrounding coolant, heat-generating particle power, and accumulated fast neutron fluence which can degrade the thermal conductivity of the matrix material in the pebble.

The following provides a general description of the response of the TRISO particle to neutron irradiation (Reference 7). Neutron irradiation of a TRISO-coated particle causes its kernel to expand outward and its buffer to shrink inward. In this process, the buffer stays bonded to the kernel but tends to delaminate from the IPyC layer. The PyC layers shrink early during irradiation and revert to swelling at longer irradiation times. As the buffer pulls away from the IPyC, a gap can be created between the two layers. Simultaneously, the buffer is pushed outward by the swelling kernel, reducing the size of the gap. The void volume of this buffer-IPyC gap adds to the increasing porosity of the kernel and decreasing porosity of the buffer to form a free volume that accommodates fission gases.

The PyC has different irradiation-induced strain rates in the radial and tangential directions because of its slightly anisotropic nature. At low fast neutron fluence, the PyC shrinks in both directions. The strain first reverses from shrinkage to swelling in the radial direction (at fast neutron fluences typically around 2×10^{25} n/m^2, E$_n$ > 0.18 MeV) and then in the tangential direction ($\sim 5 \times 10^{25}$ n/m^2, E$_n$ > 0.18 MeV), as described in Section 3.24.3.1.2 of Reference 7. The change in strain behavior depends on intrinsic PyC properties (i.e., density and degree of anisotropy measured by the Bacon Anisotropy Factor or BAF) and on the irradiation temperature.

During the early phases of irradiation, the shrinkage of the PyC puts the IPyC and OPyC layers into tension and creates compressive forces on the more rigid SiC layer, as long as the PyC layers remain intact. Cracking of the PyC can occur if the tensile stress in the layer reaches its fracture strength, resulting in high local stresses on the SiC layer which can lead to SiC failure. In addition to shrinkage, the irradiation-induced creep of the PyC layers offsets their shrinkage at longer irradiation times. As a consequence, some of the tensile stress in the PyC layers and some of the compressive stress in the SiC layer are relieved. Concurrently, fission gas pressure builds up in the free volume of the particle, putting the coating layers in tension as this pressure counteracts the effect of the shrinkage of the PyC layers, causing them to push or pull inward on the SiC. The IPyC, SiC, and OPyC act as structural layers to retain this pressure and also function as barriers to the migration of fission products. However, if the internal gas pressure increases enough, the tangential stress in the SiC layer can eventually become tensile. Failure is expected to occur if this stress reaches a value that exceeds the SiC fracture strength (Section 3.1.5.5) for the particle. The irradiation-induced behavior of the coating layers is shown schematically in Figure 2-3. Figure 2-4 provides a notional illustration of the general trend of the corresponding induced stress in the IPyC and SiC layers as a function of fast neutron fluence.

The dimensional changes of the SiC layer during irradiation are insignificant compared with the shrinkage, swelling, and creep of the IPyC and OPyC layers (Section 7 of Reference 39). Consequently, the SiC response is mostly elastic. Although some swelling of the SiC layer is anticipated during irradiation, its

magnitude is small compared to the dimensional changes of the PyC layers and it has not been observed to impact the mechanical integrity of the TRISO particle.

Design basis events for thermal hydraulic accidents in the KP-FHR are expected to be relatively mild with fuel particle temperatures well below the temperatures of the AGR program safety tests. The AGR "safety testing" was performed in dry helium at isothermal temperatures of 1600°C, 1700°C, and 1800°C for durations of approximately 300 hours. The results demonstrated robust particle performance (Reference 42). These temperatures are significantly higher than expected in the KP-FHR and the time frames are significantly longer than expected. This is due to the high thermal inertia of the molten salt and graphite reflectors. Also, the KP-FHR has a strong net negative reactivity coefficient and core excess reactivity is minimized by the continuous cycling of pebbles through the core. In addition, the low pressure of the KP-FHR means that rapid reactivity events such as rod ejections are not credible.

A summary of the fuel behavior described above is provided in Table 2-7.

2.2.2   Failure Mechanisms

Based on historical irradiation experience (Section 3.24.3.1 of Reference 7), the identified failure mechanisms of TRISO-coated fuel particles are:

- Pressure vessel[1] failure of spherical or aspherical particles resulting in the failure of all three coating layers
- Cracking of the IPyC layer leading to SiC failure
- Partial debonding of the IPyC layer from the SiC layer leading to SiC failure
- Kernel migration towards the SiC layer and its subsequent failure
- Chemical attack of the SiC layer by fission products or CO leading to its failure
- Thermal decomposition of the SiC layer at high temperatures
- Buffer fracture leading to cracking of undebonded IPyC

Carbon monoxide has historically been observed to play a major role in some of these failure mechanisms in UO_2-fueled TRISO particles. Although CO production is suppressed by design in UCO fuel, it is nonetheless discussed with the failure mechanisms below.

The following sections discuss each of these failure modes and whether or not they are modeled in fuel performance analysis evaluation model by adding them to KP-BISON.

2.2.2.1 CO production

Carbon monoxide is produced by the reaction of a net excess of oxygen with the carbonaceous buffer. This net excess of free oxygen originates from oxygen released during the fission process that is not consumed by the fission products that form oxide compounds, as these fission products are thermochemically incapable of binding all of the liberated oxygen (Section 3.24.3.1.1 of Reference 7).

Each [235]U fission within stoichiometric UO_2 leads to fission products that may combine with at most only 1.62 of the two oxygen atoms released (Section 3.24.3.1.1 of Reference 7). The remaining oxygen is then predominantly consumed in the oxidation of carbon from the buffer into CO gas. The amount of CO produced is a function of temperature and burnup and can be significant in UO_2-type fuels. Conversely, UCO fuel is designed such that the presence of UC and UC_2 compounds are converted to UO_2 from the

---

[1] Since the TRISO particle is designed to hold fission gases at a pressure substantially higher than the ambient pressure, it is referred to as a pressure vessel.

reaction with the liberated oxygen, thus limiting the amount of free oxygen available to form CO by reaction with the buffer. Post-irradiation examination (PIE) on AGR-1 and AGR-2, the first and second experiments of the AGR program, did not report any CO corrosion on UCO fuel irradiated up to ~20% Fissions per Initial (heavy) Metal Atom (FIMA) (which corresponds to approximately 200,000 MWD/MTU), which indicates a negligible amount of CO produced during these irradiation tests. [[

]]

2.2.2.2 Pressure vessel failure

During irradiation, fission gases are released from the kernel into a free volume provided by the porous buffer layer and the buffer-IPyC gap. The internal pressure in the TRISO particle builds up with temperature as the amount of fission gases increases in that free volume. In the case of UO2 fuel, CO contributes to the internal pressure, but, as shown in Section 2.2.2.1, CO production is minor in UCO fuel.

In KP-BISON, the SiC layer represents a thin wall of a spherical pressure vessel. Failure of the SiC is assumed when the tangential tensile stress induced in the SiC layer by the internal pressure exceeds the fracture strength of the SiC.

Asphericity affects the probability of failure by high internal pressure. In the fuel performance analysis model, aspherical particles are modeled as spheres with a flat facet. In this geometry, the asphericity is characterized by the aspect ratio defined as the ratio between the major and minor outer diameters of the aspherical particle. Because the SiC layer is the primary structural layer and fission product barrier, the asphericity is measured at the SiC level and a critical limit is specified for the SiC aspect ratio during manufacture of the TRISO particles. Under internal pressure, the faceted portion of aspherical particles incurs higher stresses than the spherical portions. The aspherical particle is assumed to be failed when the tensile stress in the tangential direction of the faceted portion reaches the fracture strength of the SiC. Section 5.3 of Reference 8 shows that ellipsoidal asphericity leads to a much smaller failure probability than the flat-faceted geometry. As a result, ellipsoidal asphericity is not included in the fuel performance analysis model.

Unlike failures caused by IPyC cracking or IPyC-SiC debonding (Section 2.2.2.3 and 2.2.2.4), which are governed by shrinkage of the PyC layers, failures caused by asphericity are caused by the internal pressure. Therefore, while failures due to cracking and debonding tend to occur early during irradiation when shrinkage stresses are maximum, failures due to asphericity are likely to occur later at higher burnups when the internal pressure is highest.

During irradiation of the KP-FHR fuel, the internal pressure will vary proportionally with temperature (ideal gas law) and burnup (fission gas inventory), but this pressure increase is expected to lead to a low failure probability, mainly affecting highly aspherical particles. This results from the optimized design of the TRISO particle that can accommodate fission gas up to burnups of ~20% FIMA, even at relatively high operating temperatures (~1300°C), as confirmed by the AGR-1 test (Tables 5, 6, and 7 of Reference 44). During normal operation or transients at higher temperature or during postulated accidents, the internal pressure will rise with increasing temperature and gas inventory. It is expected that there will be sufficient margin to accommodate the additional internal pressure without appreciably increasing the probability of failure by over-pressure.

2.2.2.3   IPyC cracking

Cracking of the IPyC layer occurs when irradiation-induced shrinkage of the IPyC induces a tangential tensile stress that exceeds the fracture strength in that layer. A radial crack then develops in the IPyC layer and creates local tensile stress in the SiC layer, possibly leading to the failure of the SiC if this tensile stress exceeds its own fracture strength.

Although IPyC cracking is not uncommon – reaching probabilities of a few percent under certain irradiation conditions, it does not necessarily translate into mechanical failure of the SiC layer. SiC failure depends on the magnitude of the induced tensile stress in the SiC as compared to the SiC fracture strength. On the other hand, IPyC cracks open pathways for fission products to reach the SiC layer and chemically attack it (see Section 2.2.2.6), which can lead to failures.

2.2.2.4 IPyC-SiC debonding

IPyC-SiC debonding refers to the detachment of the weakly bonded IPyC and SiC due to tensile stress generated at the interface between the layers brought on by irradiation-induced IPyC shrinkage. Debonding occurs when the radial tensile stress at the interface exceeds the bond strength between the two layers.

The debonding process is a progressive partial unzipping of the two layers that starts at a weak initiation point on their interface and then develops during irradiation. The tensile stress concentrations that occur at the interface along the debonded path are typically not as severe as those at the crack tip of a cracked IPyC (Section 2.2.2.3) but they affect a larger portion of the SiC surface.

Debonding between the IPyC and SiC layers is facilitated by a weak bond between the layers. With a low bond strength, the layers readily debond but the stress level leading to debonding is low and results in a low probability of SiC failure. Similarly, with a high bond strength, the radial stress between the layers may not be sufficient to overcome the bond strength which, again, results in a low probability of SiC failure by debonding (Section 5.2 of Reference 9). Debonding between the IPyC and SiC layers has been observed in previously U.S.-fabricated TRISO fuel (Section 5.1 of Reference 9). However, IPyC-SiC debonding was not observed in German TRISO fuel, which indicates a strong bond between the two layers. Consequently, because current U.S. TRISO particle fabrication is based on historical German processes, the IPyC-SiC bond strength is assumed to be fairly high and IPyC-SiC debonding is not expected to occur in otherwise intact particles. Furthermore, debonding between the IPyC and SiC layers has not been observed as a stand-alone failure mechanism during PIE on AGR-1 and AGR-2 UCO fuels. On the other hand, IPyC-SiC debonding has been observed at the tip of IPyC cracks, resulting in tangential cracks forming in the SiC (Section 3.4.1.2 of Reference 10). These cracks curved back into the SiC layer and do not appear to have jeopardized the integrity of the SiC layer as a fission product barrier.

[[

]]

2.2.2.5 Kernel migration

Kernel migration, also called the "amoeba effect," is the tendency of the kernel to migrate up a macroscopic temperature gradient. The kernel is pushed towards the hot side of the TRISO particle by carbon dioxide (CO_2) and solid-phase carbon (C) produced on the cold side of the particle by carbon monoxide (CO) migrating down the temperature gradient and reacting as $CO+CO\rightarrow CO_2+C$. The particle is assumed to fail when the kernel comes into contact with the coating layers.

[[

]]

2.2.2.6 Chemical attack of SiC

The SiC layer can be chemically attacked by:

- Noble metals
- Lanthanides / rare-earth elements
- Carbon monoxide

Noble metals can be transported from the kernel to the inner surface of the SiC (Section 3.24.3.1.5 of Reference 7). Palladium has been observed as a major contributor to the attack and penetration into the SiC layer, migrating to the layer and threatening its integrity by reacting with the SiC to form palladium silicides. As noted in Section 3.24.3.1.5 of Reference 7, "although the quantity of Pd is small compared with the mass of the SiC layer, the reaction is highly localized and may lead to a complete penetration of the SiC layer for longer times at high temperatures". Recent observations during AGR-1 PIE have shown that palladium corrosion of the SiC is not a widespread phenomenon and that it may only lead to SiC failure when IPyC cracks open a pathway for palladium to locally concentrate at the IPyC-SiC interface (Section 6.1.4 of Reference 10). Nevertheless, a model for palladium penetration is included in the fuel performance analysis model (Section 3.2.7).

Conversely, lanthanide and rare-earth fission products are strongly retained in UO_2 where they form stable and low-mobility oxide compounds (Reference 11). Adequate chemistry control in the fabrication of UCO fuel ensures sufficient UO_2 phase, relative to the UC and UC_2 phases, to allow oxidation of these fission products and mitigate their potential attack and corrosion of the SiC layer. Consequently, chemical attack of the SiC by lanthanide and rare earth fission products is not modeled in the fuel performance analysis model.

In addition, CO has been observed to corrode SiC in UO_2 fuel at high temperatures once the IPyC layer has lost its protective function (Section 4.2 of Reference 12). [[

]]

2.2.2.7 Thermal decomposition of SiC

SiC thermally decomposes back into its constituent elements when exposed to sufficiently high temperatures for a long duration of time. Silicon vapor then migrates out of the SiC coating, leaving behind a porous carbon layer which is not retentive of fission products.

Although initial signs of porosity in the SiC were observed at 1800°C, SiC decomposition primarily occurs above 2100°C (Reference 13). These temperatures are significantly higher than the normal operating and anticipated accident temperatures of KP-FHR, [[
]]

2.2.2.8 Cracking of partially debonded IPyC

PIE on UCO fuel irradiated by the AGR-1 and AGR-2 experiments identified a mechanism responsible for a few observed SiC failures. Instead of the expected full delamination between the buffer and IPyC layers, some AGR TRISO particles exhibited partial delamination, or no delamination at

all, between the buffer and IPyC layers (Section 3.4.1.2 of Reference 10). This partial debonding might have resulted in sufficient stress in the IPyC layer to cause its fracture. In some cases, fractures appeared in the partially (or fully) bonded buffer and propagated directly into the IPyC layer. Although buffer fracture or incomplete delamination from the IPyC rarely resulted in IPyC cracking, evidence from ceramography of AGR-1 particles suggests that strong bonding between the buffer and IPyC increases the likelihood for IPyC cracking. If IPyC cracking subsequently occurs, it opens a pathway for fission products to reach the SiC layer and degrade it. Particles with failed SiC showed evidence that cracked IPyC had exposed the inner surface of the SiC and allowed buildup of fission products that chemically degraded the SiC structure (Section 6.2 of Reference 10).

However, ceramography on irradiated AGR-2 fuel has not uncovered through-layer IPyC fractures (Section 6 of Reference 14). This lack of full IPyC fracture might result from a longer fluidization time between deposition of the buffer and IPyC layers during AGR-2 fuel particle fabrication compared to AGR-1. This longer fluidization period may weaken the buffer-IPyC bond and allow the buffer to detach more easily from the IPyC layer during irradiation. Therefore, complete delamination along the buffer-IPyC interface, which appears to be advantageous, can be achieved with an optimized fuel fabrication process.

[[

]]

2.2.2.9 Summary of TRISO Fuel Failure Mechanisms

A summary of the fuel failure mechanisms is provided in Tables 2-8 and 2-9, showing those that are modeled in the fuel performance analysis model (Table 2-8) and those that are not significant and, therefore, not modeled (Table 2-9).

2.3 PHENOMENA IDENTIFICATION AND RANKING TABLES

Key phenomena associated with the irradiation of TRISO-coated fuel particles embedded in an annular pebble have been identified and assessed for importance using the Phenomena Identification and Ranking Table (PIRT) process (as outlined in RG 1.203). The importance level of each phenomenon was assessed with regards to the mechanical integrity of the TRISO particles or fuel element (i.e., pebble) and potential release of fission products to the coolant, using (H)igh, (M)edium, and (L)ow grades. The state of knowledge relative to each identified phenomenon was also ranked, which allowed determination of any gaps and identification of actions to close these gaps, if necessary. The PIRT was also used to assess the adequacy of existing modeling tools and methods to predict the identified phenomena.

Phenomena identified with a high importance (H) or a combined medium (M) importance and low (L) knowledge levels are discussed in Table 2-10 (normal operation and AOOs) and Table 2-11 (postulated accidents). The "PIRT comments" column provides the rationale identified by the PIRT panel to take the specific phenomena into consideration. The "Modeling" column details how the phenomena are modeled in KP-BISON or provides justification for the absence of associated models.

[[

]]

[[

]]

A significant amount of PIE on AGR-1 and AGR-2 irradiated fuel has deepened the knowledge about TRISO performance during normal operating or accident conditions. The PIRT exercise performed by Kairos Power is based on the improved understanding and new information resulting from this extensive PIE work. [[

]]

2.4   FISSION PRODUCT TRANSPORT

2.4.1   Radioisotopes of Interest

Fission produces a wide array of radioisotopes, most of which have very short half-lives or form low-mobility oxide compounds in the fuel kernel. These radionuclides are generally excluded from fission product transport analysis since they do not get released from the kernel. Due to decay effects on fission product transport and the ability to diffuse through the layers of a coated particle, radiologically important fission products released from fuel elements are divided into relatively short-lived gaseous (Section 3.2.8) and long-lived metallic (Section 3.2.9) fission products.

Historically, the list of radioisotopes of interest for TRISO fuel was established by considering only the radiologically most significant isotopes to High Temperature Gas Reactor (HTGR) safety analysis studies (Table 4.2 of Reference 40). The key radioisotopes were selected based on a combination of their fission yields, their transport and release properties, and their radiological hazard significance.

During HTGR normal operations or accident conditions, the key radioisotopes consist of the long-lived strontium (^{90}Sr), silver (^{110m}Ag), cesium (^{134}Cs, ^{137}Cs), and krypton (^{85}Kr) isotopes, and the short-lived iodine (^{131}I) and xenon (^{133}Xe) isotopes. Isotopes of the same chemical species were assumed to result in the same release fractions (Section 3.24.4.1 of Reference 7). Some release characteristics of these radioisotopes under HTGR conditions are given below:

*   Silver is released from TRISO fuel at temperatures above 1000°C. It plates out at temperatures lower than ~800°C on metallic surfaces and at ~900°C on graphite. Consequently, silver represents an occupational hazard during maintenance, but it is not considered to be an offsite radiological hazard.
*   Cesium is released from TRISO particles with defective or failed SiC layers under normal HTGR operating conditions. AGR-1 PIE showed some cesium retention in the matrix, although release from the matrix occurred at HTGR accident temperatures (Section 3.2.3.1 and Section 4.5 of Reference 10).

- Strontium is fairly well retained in uranium dioxide or oxycarbide kernels at HTGR normal operating temperatures, even when the outer coating layers are defective or failed. It is also retained by the matrix, but it is slowly released at HTGR accident temperatures (Sections 3.2.3.3 and 4.5 of Reference 10).

- Iodine, krypton, and xenon share similar transport behavior and have historically been grouped together. They are retained by the PyC and SiC layers under normal operating conditions.

- The combination of [85]Kr and ^{137}Cs data allows the determination of both through-coating (full) failures and SiC failures as Cs release indicates SiC failure and Kr release indicates PyC and SiC failure.

Figure 2-5 shows an overview of the significant fission product releases that are important in the KP-FHR fuel and that will be modeled in the fuel performance analysis model.

A specific list of radioisotopes of importance to calculating dose consequence for the KP-FHR will be provided in a separate topical report on the KP-FHR Mechanistic Source Term Topical Report (Reference 15).

2.4.2 Fission Product Transport Phenomena

The transport of mobile fission products through a TRISO particle is a complex process that depends on the microstructure of the fuel materials and could involve several mechanisms such as lattice diffusion, grain boundary diffusion, pore diffusion, nano-cracking, and vapor transport (Reference 43). Furthermore, effects like irradiation-induced trapping and adsorption, thermal decomposition of the coating layers, or chemical attack of these coating layers by other fission products such as palladium or rare earth elements could potentially impact these transport mechanisms.

Moreover, different mechanisms are likely responsible for the transport of gases and metals in the different TRISO coating layers. Gaseous transport can be described using pressure driven diffusion models through porous media, but the use of these models requires information on the connected porosity, the characteristic size of the porosity, and the tortuosity of the porous media which are not well known for TRISO coating layers. For metallic fission products, a combination of grain boundary diffusion (at low temperature) and bulk diffusion (at high temperature) has been postulated.

In a fully intact TRISO-coated particle, fission products that are formed in the kernel have to be transported through the PyC and SiC layers before being diffused through the matrix and released into the coolant. The PyC layers form an effective barrier to noble gas release but do not offer significant retention to the release of metallic fission products like silver, cesium, or strontium. On the other hand, the SiC layer is the major fission product barrier in the TRISO particle and effectively retains metallic fission products with the exception of silver. Consequently, the transport rates of gaseous or metallic fission products (except Ag) are extremely slow.

Nevertheless, even under the most stringent manufacturing conditions, a small fraction of the coated particles will be defective from the manufacturing process. Furthermore, a small additional fraction could fail under irradiation or at accident temperatures. Failed particle layers from manufacturing or from postulated operating conditions result in one or more leaking coating layers that cannot fully retain fission products. In the fuel performance analysis model, a defective or failed layer is conservatively modeled by a non-retentive material with high diffusivity. In the case of a TRISO failure (i.e., defective or failed SiC and both PyC layers), the particle is represented by a bare kernel, also known as "exposed kernel". Since no credit is taken for fission product retention in the buffer, fission products in a TRISO particle with exposed kernel have only to escape the kernel to be released to the matrix material. In the absence of the defective

or failed PyC and SiC layers, the kernel remains the only part of the TRISO particle that takes credit for fission product retention.

Fission product transport is modeled by Fick's laws of diffusion. The diffusion coefficients used in the model are implicitly defined as "effective", implying that they describe the overall fission product transport using classical Fickian diffusion (Section 3.24.4.3.1 of Reference 7). In particular, this means that the application of these effective diffusion coefficients will result in the same fractional release of fission products from the TRISO particle as was observed in the integral release measurements from which they were derived.

Additionally, the large thermal gradients present in the buffer can lead to thermal diffusion (Soret effect), which should theoretically be added to the concentration-driven Fickian diffusion used to model fission product transport across the layer. Studies have been conducted on the Soret effect up to high particle powers (600 mW/particle) using a conservative value of heat of transport (Section 3.2 of Reference 16). [[

]]

3   FUEL MODELING – MATERIAL PROPERTIES AND PHYSICAL MODELS

This section describes the material properties and physical models that are to be incorporated into KP-BISON to model the KP-FHR TRISO fuel. These properties and models were selected from those used historically for HTGRs and are judged to be applicable to the KP-FHR fuel design. In some cases, the properties and models are outside the range of applicability for which they were developed. In these cases, the properties are determined by extrapolation. In other cases, they were developed for UO_2 rather than UCO or for different geometries than the spherical KP-FHR fuel design. To address this, sensitivity analyses will be performed for each of these properties and models to ascertain how important the properties are to the fuel performance results. It is expected that many of these will have a minor impact on results. For those that are shown to significantly influence the results, conservatisms will be applied. In addition, as part of the validation process, fuel performance analysis results using these properties and models in KP-BISON will be compared to failure data from AGR-1, AGR-2, and other selected data from experiments such as AGR-5/6/7 to confirm that the selected properties and models produce conservative predictions of fuel failure rates. (OPEN ITEM)

3.1   MATERIAL PROPERTIES

The applicability range of the material properties is summarized below (Section 7.1.1 of Reference 20):

- The level of fast neutron fluence accumulation is limited to the range $0.1 – 3.96 \times 10^{25}$ n/m^2 ($E_n >$ 0.18 MeV) and the range of irradiation temperatures is 600 – 1300°C in general; irradiation conditions outside of these ranges are not fully covered due to the lack of available experimental data.
- The densities are limited to 1.8 – 2.0 g/cm^3 for dense PyC (IPyC and OPyC layers) and 0.9 – 1.1 g/cm^3 for porous PyC (buffer); the density of the SiC is > 3.18 g/cm^3.
- The material properties for the buffer are extrapolated from the PyC to lower densities which can affect the accuracy of the predictions on buffer behavior.

It is assumed that the effects of multiple parameters (e.g., temperature, fast neutron fluence, density, etc.) are mutually independent and their combined effect can be obtained by multiplying them together. When the dependence of material properties (e.g., Poisson's ratio) on some of the parameters is unknown, the material properties are assumed to be independent of these parameters.

Material properties are described for the kernel, the buffer, the pyrolytic carbon, the buffer-IPyC gap, the silicon carbide, and the matrix. [[

]]

3.1.1   Kernel Material Properties

The kernel is the heat source of the TRISO particle and, by extension, of the fuel element and the KP-FHR core. It contains the fissile material in the form of UCO and is the source of fission products whose transport to the coolant is limited by the three outer coating layers. Legacy TRISO fuel development programs have predominantly focused on UO_2 fuel and, consequently, most kernel properties are based on UO_2 experimental data. These properties and their treatment in the fuel performance analysis model are discussed below.

3.1.1.1 Kernel Swelling

Kernel swelling occurs throughout irradiation as solid and gaseous atoms released by fission accumulate in the kernel, resulting in a volume increase of the kernel. In a TRISO particle, this volume increase is accommodated by the porous buffer layer. However, under extreme conditions, swelling can lead to the mechanical interaction of the kernel with the outer coating layers which may result in particle failure. [[   ]]

Solid Swelling

Solid fission products constitute about 75% of the fission products, or ~150 atoms for 100 actinide atoms fissioned. Of the remaining 50 atoms, about half are noble gases (mainly Kr and Xe isotopes) and the other half are volatile fission products (e.g., Br, Cs, I, or Rb). Solid swelling occurs as every lattice site vacated by one fissioned actinide must accommodate ~1.5 solid fission products and volatile fission products in solid solution or that form solid compounds (e.g., CsI).

Experimental data indicate a strong dependence of kernel swelling on burnup, as expected from theoretical considerations. [[

                                                                                    ]]

Gaseous Swelling

Gaseous swelling results mainly in an increase of bubble population and size in the fuel lattice and at its grain boundaries. Complex mechanisms drive gaseous swelling and models are often based on empirical correlations depending on a number of parameters of which temperature and burnup are the most important.

[[

                                                                                    ]]

Kernel Swelling in KP-BISON

The volumetric change in kernel volume, or swelling S (-), is given by:

[[

]] This experimental result was obtained based on limited statistics and will be confirmed by AGR-2 PIE measurements. (OPEN ITEM)

3.1.1.2 Densification

In LWRs, sintered UO_2 densifies at the beginning of irradiation as thermal and fission spikes (localized high-energy deposition by fission fragments) collapse the finer porosity. Empirical models have been developed to describe the densification of the LWR sintered fuel. As TRISO fuel produced to high density (>95% of theoretical density) by a sol-gel process can have a different size distribution of its porosity, these models do not apply to predict its densification (Section 1.2 of Reference 16). [[

]]

3.1.1.3 Elastic Properties

Elastic properties of UO_2 are used in KP-BISON.

Elastic Modulus

[[

]]

Poisson's Ratio

[[

]]

$$\mu = 1.35 \times \frac{1.92 \times \rho - 0.92 \times \rho_{th}}{1.66 \times \rho - 0.66 \times \rho_{th}} - 1 \qquad \text{(Eq. 4)}$$

[[

]]

3.1.1.4 Thermal Conductivity

[[

]]

3.1.1.5 Heat Capacity

[[

]]

3.1.1.6 Thermal Expansion

[[

]]

3.1.2 Buffer

The buffer is a porous carbon layer that accommodates kernel swelling and fission gases to limit over-pressure in the TRISO particle. Its properties are similar to PyC (Section 3.1.3) but applied at a lower density and for an isotropic material. The treatment of buffer properties is described below.

3.1.2.1 Elastic Properties

Elastic Modulus

[[
]]

[[

]]

Poisson's Ratio

[[

]]

3.1.2.2 Irradiation-induced creep

Pyrocarbon undergoes creep (inelastic strain) during irradiation and under stress at temperatures where thermal creep is considered negligible (and, therefore, not modeled). Although transient creep impacts the stress level in the TRISO coating layers early in irradiation, its modeling parameters are not well established. Furthermore, transient creep affects fuel failure much less significantly than steady-state creep (Reference 22). [[

]]

Creep Coefficient

[[

]]

Poisson's Ratio in Creep

[[

]]

3.1.2.3 Irradiation-induced Dimensional Change

When pyrocarbon is irradiated, energetic knock-on carbon atoms are displaced from the lattice by colliding fast neutrons. The recombination of the displaced atoms and vacancies result in the formation of loops or in their annihilation at structural defects. The competition of various sinks for these point defects creates a complicated pattern of dimensional changes in the crystallites that lead to macroscopic changes in the dimension of the pyrocarbon

Under irradiation, isotropic pyrocarbon (e.g., the buffer) shrinks early and then reverses to swelling. Anisotropic pyrocarbon (e.g., PyC) initially shrinks in both the parallel and perpendicular directions before reversing to swelling at a low turn-around fast neutron fluence for the perpendicular direction and at a high turn-around fast neutron fluence for the parallel direction. The shrinkage or swelling of the

[[

]]

3.1.2.4 Thermal Conductivity

[[

]]

3.1.2.5 Specific Heat Capacity

[[
]]

[[

]]

3.1.2.6 Thermal Expansion

[[

]]

3.1.3 Pyrolytic Carbon (PyC)

The PyC layers act as secondary structural layers and fission gas barriers in the TRISO particle. The material properties of PyC are complex and strongly dependent upon the coating conditions under which it is deposited. In particular, the PyC coatings are anisotropic although the goal is to minimize the degree of anisotropy. Consequently, the key material properties are directionally dependent. The treatment of the PyC layer in the fuel performance analysis model is described below.

3.1.3.1 Elastic Properties

Elastic moduli

[[

]]

Poisson's ratio

[[   ]]

[[

]]

3.1.3.2 Irradiation-induced Creep

Creep coefficient

[[

]]

Poisson's Ratio in Creep

[[

]]

3.1.3.3 Irradiation-induced Dimensional Change

[[

]]

[[

]]

[[

]]

Under high strain, reorientation of the PyC crystallites parallel to the IPyC-SiC interface leads to higher anisotropy (Reference 41). This increase of BAF with fast neutron fluence leads to higher stresses and the potential for particle failure at high fast neutron fluences. [[

]]

3.1.3.4 Thermal Conductivity

[[

]]

3.1.3.5 Specific Heat Capacity

[[

]]

3.1.3.6 Thermal Expansion

[[

]]

3.1.3.7 Weibull Characteristic Strength and Modulus

[[

]]

[[

]]

3.1.4 Buffer-IPyC Gap

As irradiation progresses, the buffer shrinks inward and debonds from the IPyC, forming a gap that fills up with fission gas and creates the largest thermal resistance in the TRISO particle. The treatment of the buffer-IPyC gap in the fuel performance analysis model is described below.

3.1.4.1 Heat Transfer

Heat produced in the kernel is transferred to the outer coating layers through the buffer-IPyC gap via a gap conductance model using the width of the gap and the conductivity of the gas mixture (Kr and Xe) in the gap. [[

]]

[[

]]

[[

]]

[[

]]

3.1.5 Silicon Carbide (SiC)

The SiC layer is the primary structural layer and primary fission product barrier in the TRISO particle. The material properties of SiC are strongly dependent upon the coating conditions under which it is deposited. High-quality SiC coatings are near theoretical density and are assumed to behave isotropically.

The behavior of the SiC layer in TRISO particles is essentially elastic. [[

]]

3.1.5.1 Elastic Properties

Elastic Modulus

[[

]]

3.1.5.2 Thermal Conductivity

[[

]]

3.1.5.3 Specific Heat Capacity

[[

]]

3.1.5.4 Thermal Expansion

[[

]]

3.1.5.5 Weibull Characteristic Strength and Modulus

SiC is a brittle material and, as such, its probability of failure is calculated using Weibull statistics. [[

]]

3.1.6   Matrix

The matrix serves as the medium between the coolant and the TRISO fuel particles. Its temperature locally sets the boundary condition for thermal profile calculation in the TRISO particles and, conversely, the fission products released from the particles provide a source term for the pebbles to assess fission product release to the coolant. [[

]]

3.1.6.1 Irradiation-induced Dimensional Change

Despite evidence of irradiation-induced shrinkage of the matrix in the AGR-1 and AGR-2 experiments (Reference 26 and Reference 27), no deleterious effect, such as OPyC fracture, has been observed in PIE (Sections 3.3 and 4.3.3 of Reference 28 and Reference 14). Furthermore, the low magnitude of the shrinkage (~1%) has no impact on the thermal state of the fuel element. [[

]]

3.1.6.2 Thermal Conductivity

The thermal conductivity of the matrix depends on its material composition, final heat treatment temperature, irradiation temperature, accumulated neutron fluence, and density. In the case of the fueled zone of the pebble (fuel annulus), it also depends on the packing fraction, i.e., the volumetric ratio of the TRISO particles to the embedding matrix. The thermal conductivity of the unfueled matrix, k_m (W/m-K), is given by:

[[

]]

[[
]]

[[

]]

3.1.6.3 Specific Heat Capacity

[[

]]

[[

]]

3.2   PHYSICAL MODELS

The treatment of physical phenomena models in the fuel performance analysis model is described below.

3.2.1   Strain-Displacement and Stress-Strain Constitutive Relationships

[[

]]

3.2.2   Failure Probability

[[

]]

[[

]]

3.2.3   Heat Equation

[[

—

]]

3.2.4   Fission Yields

The numbers of fission product atoms created per fission, or fission yields, for Ag, Cs, Sr, and noble gases (Kr + Xe) depend on the neutron spectrum in KP-FHR. Fission yield correlations taking into account the spatial variation of the neutron spectrum throughout the KP-FHR core [[
]]

3.2.5   Fission Gas Release (long-lived isotopes)

The release process of fission gas from the kernel is relatively complex, but it can be described as a two-step process: in the first step, the gas atoms are driven through the grain towards the grain boundary; in the second step, the gas atoms migrate from the grain boundary to the free surface of the

fuel where they are instantaneously released into the free volume. Fission gas release of long-lived isotopes from the kernel is modeled through recoil and diffusion to grain boundaries. For both phenomena, the model calculates a release fraction, RF (-), which corresponds to the fraction of the gas generated by fission that is released by the kernel. The combined release of long-lived fission gas is given by:

[[

]]

Booth Equivalent Sphere Diffusion

Diffusive release through grains to the grain boundaries and subsequent transport through the interconnected porosity is estimated by the Booth equivalent sphere diffusion model. [[

]]

[[

]]

[[

]]

[[

.

]]

3.2.6   Internal Gas Pressure

Fission gas released from the kernel accumulates in the void volume of the particle (porosities in the kernel and buffer plus the volume of the buffer-IPyC gap) where it builds up the internal pressure. The pressure, P (Pa), is calculated using the [[

]]

[[

]]

3.2.7   Palladium Penetration

Fission product palladium is known to attack SiC at localized reaction sites. The fission yield of palladium is higher in ^{239}Pu than in ^{235}U or ^{238}U by a factor of 25-50, so the high-assay low-enriched-uranium (HALEU) TRISO fuel of the KP-FHR will produce more palladium than the conventional low-assay LEU LWR fuel. Consequently, the potential for attack and penetration of palladium into the SiC layer exists. However, based on the international historical database, the penetration rate of palladium into SiC has been found to have an Arrhenius temperature dependence and it is limited at temperatures lower than 1000°C.

[[

]]

3.2.8   Release Rate to Birth Rate Ratios (short-lived isotopes)

The release of short-lived gaseous isotopes from nuclear fuel is expressed as a release rate to birth rate ratio, R/B (-), which represents the ratio between the rate at which the isotope is released from the fuel (R) and the rate at which the isotope is produced in the fuel (B). In the case of TRISO fuel particles, the R/B of short-lived fission gas (Kr and Xe) isotopes has two components: uranium contamination (dispersed uranium outside of the SiC layer, i.e., in the OPyC or matrix) and exposed kernels (as-fabricated defective particles or particles fully failed during irradiation). [[

]]

Uranium Contamination

[[

]]

<u>Exposed Kernels</u>

[[

]]

The decay constants of the short-lived krypton and xenon isotopes produced in TRISO fuel particles are given in Table 3-7.

3.2.9   Fission Product Transport

The transport of mobile fission products through a TRISO particle is modeled by Fick's laws of diffusion using effective diffusion coefficients (Section 2.4.2).

Historically, PIE on irradiated TRISO fuel has primarily detected and measured the release of the following radionuclides (Section 2.4.1): silver, cesium, krypton, and strontium. Iodine and xenon have also been observed, with similar behavior as krypton. An international database has been assembled by the International Atomic Energy Agency (IAEA, see Appendix A of Reference 35) and serves as a reference for fission product transport modeling codes. The diffusivities of other radioelements (barium, cerium, europium, and ruthenium) have been measured in some of the components of TRISO particles (kernel or coating layers), resulting in either incomplete datasets or in diffusing times larger than the in-reactor residency time of the fuel. Consequently, the fuel performance analysis model currently includes models of the transport of fission products Ag, Cs, Sr, and Kr. I and Xe are assumed to have the same release behavior as Kr (Appendix A of Reference 35).

Fission product transport through the TRISO particle neglects sorption or trapping of fission products within a coating layer. As a consequence, discontinuities in fission product concentration at the interfaces are not modeled, and the partition coefficients are set to 1.

With these assumptions, fission product transport is modeled with the following set of equations:

[[

]]

3.3   SUMMARY

A summary and description of the material properties and the physical models incorporated in the fuel performance analysis model is provided in Table 3-9 and Table 3-10, respectively.

4   VERIFICATION AND VALIDATION

Verification is the process of ensuring that an analysis code mathematically produces the correct answers on the computer that it resides on. Verification involves running standardized sample problems to confirm that the computer code when installed on the user's computer produces the established sample problem output. Validation is the process of ensuring that the analytical code and models produce results that align with results from experiments and testing. Validation is usually performed using comparison with test data or comparisons with other computer codes.

This section describes the verification and validation (V&V) for the KP-BISON code. In addition, the section discusses uncertainty analysis including uncertainty quantification and sensitivity analysis. The purpose is to develop a methodology for code and solution verification, validation of physics-based models using experimental data, characterization of the potential uncertainties in these data, and evaluation of uncertainty due to potential model inadequacy.

The KP-BISON V&V will be performed in accordance with the applicable elements of the Kairos Power Quality Assurance Program.

4.1.1   Verification

To support use in fuel performance calculations, each module (material property, physical model, etc.) in KP-BISON is tested by individual unit and regression tests that are part of an extensive test matrix included with the BISON source code. These tests ensure the modules compute the correct analytical or known solutions and that they perform identically after changes are made to the code.

The verification process of KP-BISON also includes an evaluation of mesh, temporal convergence and solver tolerance. Mesh refinement defines the choice between coarse and fine meshes to model the different regions of the TRISO particle and pebble. [[

]]

In addition to the aforementioned tests, KP-BISON is subjected to the exercise of code-to-code benchmarking on sample cases specific to TRISO fuel performance. The sample cases include:

- Comparison to the TRISO fuel performance code PARFUME (Reference 20) on select cases representative of KP-FHR operating and accident conditions.

- Cases 1 to 13 of the IAEA Coordinated Research Program (CRP)-6 benchmark on fuel performance models during normal operation and operational transients conducted by the IAEA CRP on "Advances in High Temperature Gas Cooled Reactor Fuel Technology" (Reference 36).
- Cases 1 to 5 of the IAEA CRP-6 benchmark on fission product release behavior models under accident conditions (Reference 36).

4.1.2 Validation

Validation of the TRISO fuel performance model is primarily performed on an integral basis based on the failure data and release of fission products data from testing. The emphasis on integral effects testing is due to the challenges with setting up experiments that can study separate effects in a way that is representative of the full system of the TRISO fuel particles and surrounding fuel element. The KP-BISON TRISO model is developed to provide an accurate and conservative assessment of fuel integrity and leak-tightness. Therefore, validation of the model is aimed at confirming the predictions of TRISO fuel failure probability and fission product release envelop corresponding experimental data. There is some validation based on separate effects tests which is discussed in Section 4.1.2.3. Validation of KP-BISON is performed by comparing computed results to particle failure and fission product release data from experiments and by performing code-to-code benchmarks.

4.1.2.1 Comparison Against Experimental Data

The following experimental results are used for validation of the KP-BISON fuel performance model:

- AGR-1 and AGR-2 experimental data not covered by international benchmarks but that are relevant to KP-FHR irradiation conditions
- Experimental data from irradiation at the High Flux Reactor (HFR) irradiation and safety testing at the KuhlFinger Apparatur - (KüFa)
- Experimental data from the Chinese HTR-PM irradiation and safety testing campaigns
- Selected data from AGR-5/6/7 experimental results

4.1.2.2 Code-to-code Benchmarks

The following code-to-code benchmarks are performed using KP-BISON:
- Cases 6 to 11 of the IAEA CRP-6 benchmark on fission product release behavior models under accident conditions (Reference 36).
- Gen-IV benchmark on TRISO fuel performance models under accident conditions (Reference 49).

4.1.2.3 Separate Effects Validation

[[

]]

[[

]]

Validation against experimental data related to fuel temperature is performed with data from experiments at the following facilities:

[[

]]

4.1.3   Uncertainty Quantification

4.1.3.1   Overview

[[

]]

[[

]]

4.1.3.1.1 Fuel Manufacturing Properties

[[

]]

[[

]]

[[

]]

[[

]]

[[

]]

[[

]]

[[

]]

4.1.4   Sensitivity Analysis

[[

]]

4.1.5   Validation, Verification and Uncertainty Quantification Results

The results of the Validation, Verification, and Uncertainty Quantification for KP-BISON will be determined and addressed with documentation provided or referenced with an application for an operating license for a KP-FHR. (OPEN ITEM)

5   KP-BISON CODE

5.1   CODE DESCRIPTION

BISON is an engineering-scale multi-dimensional finite-element based nuclear fuel performance code (Reference 3). The code can be applied to a variety of fuel forms including LWR pellets and fuel rods, TRISO-coated fuel particles, and metallic fuel in both rod and plate geometries. Modeling of these fuels is available in 1D-spherical, 2D-axisymmetric, or 3D geometries for both steady-state and transient fuel behavior and reactor operations.

The governing equations in BISON consist of fully-coupled partial differential equations for energy conservation (heat conduction equation including energy generation by fission), species conservation (Fick's laws of diffusion including radioactive decay), and momentum conservation (Cauchy momentum equation). BISON also includes constitutive models for both nonlinear kinematics (which is suitable for large deformation) and nonlinear material behavior.

Constitutive models implemented for UCO fuel are fission product swelling, elastic properties (Young's modulus and Poisson's ratio), thermal properties (thermal conductivity and specific heat capacity), and fission product (solid and gas) generation and release. For the buffer and PyC layers, elastic properties (Young's modulus and Poisson's ratio), irradiation-induced creep properties (creep coefficient and Poisson's ratio in creep), anisotropic irradiation-induced strain, and thermal properties (thermal conductivity, specific heat capacity, and thermal expansion) are included. The thermal conductivity of the fission gases is modeled to take into account heat transfer in the buffer-IPyC gap, which is simulated using standard thermal and mechanical contact algorithms. Assuming ideal gas behavior, particle internal pressure is computed based on the evolving gap volume and fission gas release. For the SiC layer, elastic properties (Young's modulus and Poisson's ratio) and thermal properties (thermal conductivity, specific heat capacity, and thermal expansion) are modeled. Finally, elastic properties (Young's modulus and Poisson's ratio) and thermal properties (thermal conductivity and specific heat capacity) are included for the fuel matrix material. Additionally, the displacement field, which is the primary solution variable, is connected to the stress field via the strain through a constitutive relation.

BISON is built on Multiphysics Object-Oriented Simulation Environment (MOOSE) (Reference 4), a parallel, finite-element based framework that solves systems of coupled nonlinear partial differential equations using the Jacobian-free Newton-Krylov method (Reference 37). MOOSE is able to investigate computationally large problems, as is often encountered in nuclear fuel calculations. It also avoids the need for generating and inverting the Jacobian matrix, which is typically not analytically attainable and whose numerical approximation via finite-difference methods is not easily invertible.

In addition, MOOSE supports the use of complex two- and three-dimensional meshes and uses implicit time integration, which is important for the widely varied time scales in nuclear fuel simulation.

5.2   MODIFICATIONS TO BISON CODE

Modifications to BISON were made to implement KP-FHR technology specific requirements and are based on the material properties and physical models described in Section 3 of this report and are summarized in Tables 3-9 and Table 3-10. No other changes to the code or the code solution technique are made.

5.3   CODE INPUTS

The input parameters to KP-BISON consist of fuel (TRISO particle and pebble) characteristics and irradiation conditions. These are used as parameters to the material properties and physical models that KP-BISON uses to determine the thermo-mechanical state of the fuel. This mechanical state is then used to assess the integrity of the fuel barriers (failure of the coating layers) and their leak-tightness (release of fission products).

5.3.1   Fuel Characteristics

The input parameters for the fuel are given below for each of its components.

- UCO Kernel: ^{235}U enrichment (wt%), O/U and C/U ratios, density (kg/m^3), diameter (m), and average grain radius (m)

- Buffer: density (kg/m^3), theoretical density (kg/m^3), and thickness (m)

- PyC: density (kg/m^3), BAF (-), and thickness (m)

- SiC: density (kg/m^3), theoretical density (g/cm^3), thickness (m), and aspect ratio (-)

- Matrix: density (kg/m^3), thickness (m), and packing fraction (-)

- Pebble: inner core radius (m), fuel annulus thickness (m), and outer shell thickness (m)

- As-fabrication defects: dispersed uranium fraction (-), exposed kernel fraction (-), defective SiC coating fraction (-), and defective IPyC/OPyC coating fractions (-)

The KP-FHR fuel will be fabricated with tolerances around its design nominal characteristics. Because off-normal characteristics (e.g., a thin buffer or SiC layer) can lead to an increase in failure fraction, the distributions of the fuel properties are taken into account in KP-BISON by statistical sampling assuming normal distributions. This ensures that the tails of the distributions, where properties are closer to their critical limits, are correctly included in the calculation of the failure fraction are not over-represented.

5.3.2   Irradiation Conditions

The irradiation parameters required for KP-BISON are the temperature (K) of the pebble surface (boundary condition for thermal heat transfer calculations), the fission rate density (fission/m^3-s) in the kernel (used for burnup, heat generation, and fission product inventory calculations), and the fast neutron fluence ($\times10^{25}$n/m^2, E$_n$ > 0.18 MeV). These irradiation parameters are provided to KP-BISON by neutronics and thermal-hydraulics codes to inform so-called "pebble trajectories", i.e., paths followed by the fuel pebbles in the KP-FHR core. For generic fuel performance calculations, these pebble trajectories set the irradiation conditions undergone by the TRISO fuel particles as their embedding pebbles transit through the core. On the other hand, for the purpose of uncertainty quantification, the irradiation conditions will be enveloped by two fictitious low- and high-temperature bounding trajectories (Section 4.1.3.1.3).

6 FUEL PERFORMANCE ANALYSIS METHODOLOGY

6.1 OVERVIEW

The purpose of KP-BISON is to assess the structural integrity and leak-tightness to fission products of TRISO-coated UCO fuel particles under neutron irradiation in the KP-FHR core. The code allows the user to calculate the thermo-mechanical behavior of the coating layers and their potential failure (Section 6.2) as well as the potential release of fission products (Section 6.3). These calculations can be coupled or treated independently. Additionally, the TRISO particles can be modeled individually or embedded in a fuel pebble.

As described in Section 2.1, the design of the KP-FHR fuel includes TRISO particles embedded in a spherical pebble to form a fuel element. The fuel element is subject to a temperature distribution that results from the heat generated in the TRISO particles, the boundary condition imposed by the surface temperature of the pebble, and the intrinsic thermal properties of the fuel constituent materials (kernel, coating layers, and matrix material). Under thermal influence, fission products can diffuse from the fuel kernels of TRISO particles through their coating layers and into the pebble matrix and then be released from the matrix into the molten salt coolant.

[[

]]

Figure 6-1 depicts the general calculation process involving the thermal and fission product transport analyses performed by KP-BISON in the TRISO particles and pebble in the case of coupled models (Section 6.4). It can be summarized as follows:

[[

]]

[[

]]

6.2   PARTICLE FAILURE

[[

]]

[[

]]

[[

]]

The methodology for performing the 2D mapping will be provided in final revision of this topical report. (OPEN ITEM)

6.3   FISSION PRODUCT RELEASE

Fission product transport in KP-BISON follows a three-step process:

- Macro thermal analysis of the fuel element
- Micro thermal analysis and fission product transport analysis for fuel particles
- Fission product transport analysis for the fuel element

The last step ultimately leads to the release of fission products to the coolant. As noted in Section 6.1 the retention of fission products by the pebble is not being credited at this time.

[[

]]

[[

]]

6.4 COUPLING

6.4.1 Failure fraction and fission product release

[[

]]

[[

]]

[[

]]

6.5   CODE OUTPUTS

The main outputs of KP-BISON are the time-dependent fuel failure probabilities and fission product release fractions.

Specifically, the calculated failure fraction are:

- Probability of SiC failure
    - o   Contribution due to palladium penetration
    - o   Contribution due to IPyC cracking
    - o   Contribution due to pressure (including asphericity)
- Probability of IPyC cracking

The following time-dependent outputs are used to compute the main outputs and are provided for data analysis:

- Stress distributions
    - o   Radial stresses at IPyC/SiC and SiC/OPyC interfaces
    - o   Tangential stresses at inner and outer surfaces of IPyC, SiC, and OPyC layers
- Displacements and radii of kernel, buffer, buffer-IPyC gap, and outer coating layers
- Temperature distributions in kernel, buffer, buffer-IPyC gap, outer coating layers and pebble
- Fission gas inventory
- Internal gas pressure
- R/Bs
- Fission product inventory

6.6   FUEL PERFORMANCE INTERFACES

Design input is required from several sources to perform a fuel performance analysis as previously described in Section 5.3.2. Core thermal-hydraulic analyses provide the pebble surface temperature from the molten salt coolant temperature, which is the boundary condition for the fuel performance calculations. These analyses are performed using the KP-SAM code. Nuclear design input to the fuel performance evaluation is provided from the SERPENT code. The nuclear design input includes peak pebble power, power history data, fast neutron flux, and fuel pebble/particle radial power distribution. For transient calculations, the KP-SAM code is used to perform the pebble/particle power versus time and the coolant boundary conditions versus time.

The outputs of the fuel performance calculation using KP-BISON are provided ensure that the TRISO failures assumed in the source term analysis are not exceeded. Figure 6-6 provides a flow chart of the fuel performance interfaces.

6.7   LIMITS OF CODE APPLICABILITY

The use of KP-BISON is limited to ranges in TRISO fuel and pebble properties and irradiation conditions, some of which affect the TRISO material properties. These limits are based on consideration of specifications for fuel fabrication, validity ranges of the TRISO particle material properties, and ranges covered by the experimental data used to validate KP-BISON. The resulting limits of code applicability for the use of KP-BISON in analyzing TRISO fuel particles are given in Table 6-2.

In addition, KP-BISON is limited to steady state operation and the limited transient operation defined by the AGR safety testing in Section 2.2.1.

7   SUMMARY

This report describes the KP-BISON code and fuel methodology used to conduct fuel performance analysis of UCO TRISO-coated particle fuel in a KP-FHR.

The fuel performance analysis methodology provides methods to calculate the IPyC/SiC layers failure fraction and subsequent release fraction for a collection of TRISO fuel particles embedded in a KP-FHR fuel element. These analyses can be coupled or decoupled. [[

]]

The fuel performance methodology uses the KP-BISON code to perform the fuel performance analyses. KP-BISON was specifically modified to accommodate KP-FHR fuel, in particular the material properties and physical models specific to the KP-FHR design. The methodology for verification and validation are described and will be performed on KP-BISON in accordance with Kairos Power software quality assurance standards. The methodology for quantification of uncertainties in fuel performance calculations is also described.

Kairos Power requests NRC approval of the following, subject to the limitations described in Table 6-2:

- The methodology for performing fuel performance calculations.
- The methodology for determining uncertainties in fuel performance calculations.
- Use of KP-BISON computer code as described in this report is acceptable for performing fuel performance analyses for normal operation, AOOs, design basis events, and beyond design basis events.

This request for approval is subject to resolution of the following open items, which are expected to be provided in a subsequent revision of this topical report or in safety analysis report documents provided as part of licensing applications submitted under 10 CFR 50 or 10 CFR 52.

- As part of the validation process, fuel performance analysis results using the fuel properties and models in Section 3 will be compared to failure data from AGR-1, AGR-2, and other selected data from experiments such as AGR-5/6/7 to confirm that the selected properties and models produce conservative predictions of fuel failure fraction (Section 3, first paragraph).
- The experimental result on kernel swelling was obtained based on limited statistics and will be confirmed by AGR-2 PIE measurements (Section 3.1.1.1).
- The results of the Validation, Verification, and Uncertainty Quantification for KP-BISON will be determined and addressed with documentation provided or referenced with an application for an operating license for a KP-FHR (Section 4.1.5).
- The methodology for performing the 2D mapping will be provided in final revision of this topical report (Section 6.2).

8   REFERENCES

1. Kairos Power, LLC, "Design Overview for the Kairos Power Fluoride Salt-Cooled, High Temperature Reactor," KP-TR-001-P, February 2020. (ML20045E423)
2. Kairos Power LLC, "Principal Design Criteria for the Kairos Power Fluoride Salt-Cooled, High Temperature Reactor," KP-TR-003-P, June 2020. (ML20167A174)
3. R. Williamson, J. Hales, S. Novascone, M. Tonks, D. Gaston, C. Permann, D. Andrs and R. Martineau, "Multidimensional multiphysics simulation of nuclear fuel behavior," Journal of Nuclear Materials, vol. 423, pp. 149-163, 2012.
4. D. Gaston, C. Newman, G. Hansen and D. Lebrun-Grandié, "MOOSE: A parallel computational framework for coupled systems of nonlinear equations," *Nuclear Engineering and Design,* vol. 239, pp. 1768-1778, 2009.
5. D. W. Marshall, "AGR-5/6/7 Fuel Specification," Idaho National Laboratory, Report INL/MIS-11-21423 (SPC-1352) Rev. 8, March 2017.
6. G. K. Miller, D. A. Petti, D. J. Varacalle and J. T. Maki, "Consideration of the effects on fuel particle behavior from shrinkage cracks in the inner pyrocarbon layer," *Journal of Nuclear Materials,* vol. 295, pp. 205-212, 2001.
7. K. Verfondern, "TRISO Fuel Performance Modeling and Simulation," in *Comprehensive Nuclear Materials*, Elsevier Ltd, 2012, pp. 755-788.
8. G. K. Miller and D. C. Wadsworth, " Treating asphericity in fuel particle pressure vessel modeling," *Journal of Nuclear Materials,* vol. 211, pp. 57-69, 1994.
9. G. K. Miller, D. A. Petti and J. T. Maki, "Consideration of the effects of partial debonding of the IPyC and particle asphericity on TRISO-coated fuel behavior," *Journal of Nuclear Materials ,* vol. 334, pp. 79-89, 2004.
10. P. A. Demkowicz, J. D. Hunn, R. N. Morris, I. J. v. Rooyen, T. J. Gerczak, J. M. Harp and S. A. Ploger, "AGR-1 Post Irradiation Examination Final Report," Idaho National Laboratory, Report INL/EXT-15-36407, August 2015.
11. F. Homan, T. Lindemer, E. Long, T. Tiegs and R. Beatty, "Stoichiometric effects on performance of high-temperature gas-cooled reactor fuels from the U-C-O system," *Nuclear Technology,* vol. 35, pp. 428-441, 1977.
12. K. Minato, T. Ogawa, S. Kashimura, K. Fukuda and I. Takahashi, "Carbon monoxide-silicon carbide interaction in HTGR fuel particles," *Journal of Materials Science,* vol. 26, pp. 2379-2388, 1991.
13. N. Rohbeck and P. Xiao, "Evaluation of the mechanical performance of silicon carbide in TRISO fuel at high temperatures," *Nuclear Engineering and Design,* vol. 306, pp. 52-58, 2016.
14. F. Rice, J. Stempien and P. Demkowicz, "Ceramography of Irradiated TRISO Fuel from the AGR-2 Experiment," Idaho National Laboratory, Report INL/EXT-16-39462, September 2016.
15. Kairos Power, "Kairos Power Fluoride Salt-Cooled High Temperature Reactor Mechanistic Source Term," June 2020.
16. D. Petti, P. Martin, M. Phélip and R. Ballinger, "Development Of Improved Models And Designs For Coated-Particle Gas Reactor Fuels," Idaho National Laboratory for the International Nuclear Energy Research Initiative, Report INEEL/EXT-05-02615, December 2004.

17. L. J. Siefken, E. W. Coryell, E. A. Harvego and J. K. Hohorst, "MATPRO - A Library of Material Properties for Light-Water-Reactor Accident Analysis," Idaho National Laboratory for the U.S. Nuclear Regulatory Commission, Report NUREG/CR-6150 Vol. 4 Rev. 2, January 2001.

18. G. R. Bower, S. A. Ploger, P. A. Demkowicz and J. D. Hunn, "Measurement of kernel swelling and buffer densification in irradiated UCO-TRISO particles," *Journal of Nuclear Materials,* vol. 486, pp. 339-349, 2017.

19. D. R. Olander, Fundamentals Aspects of Nuclear Reactor Fuel Elements, Technical Information Center - Energy Research and Development Administration, 1976.

20. G. K. Miller, D. A. Petti, J. T. Maki, D. L. Knudson and W. F. Skerjanc, "PARFUME Theory and Model Basis Report," Idaho National Laboratory, Report INL/EXT-08-14497 Rev. 1, September 2018.

21. J. Fink, "Thermophysical properties of uranium dioxide," *Journal of Nuclear Materials ,* vol. 279, pp. 1-18, 2000.

22. G. K. Miller, "Considerations of Irradiation-Induced Transient Creep in Fuel Particle Modeling," Journal of Nuclear Science and Technology, vol. 32, no. 10, pp. 989-1000, 1995.

23. V. Barabash, I. Mazul, R. Latypov, A. Pokrovsky and C. Wu, "The effect of low temperature neutron irradiation and annealing on the thermal conductivity of advanced carbon-based materials," Journal of Nuclear Materials, Vols. 307-311, pp. 1300-1304, 2002.

24. L. L. Snead, T. Nozawa, Y. Katoh, T.-S. Byun, S. Kondo and D. A. Petti, "Handbook of SiC properties for fuel performance modeling," *Journal of Nuclear Materials,* vol. 371, pp. 329-377, 2007.

25. K. Wilcox and Q. Wang, "16.90 Computational Methods in Aerospace Engineering; Chapters 3.4.1 and 3.4.2," Massachussetts Institute of Technology: MIT OpenCourseWare, 2014. [Online]. Available:https://ocw.mit.edu.

26. P. Demkowicz, L. Cole, S. Ploger and P. Winston, "AGR-1 Irradiated Test Train Preliminary Inspection and Disassembly First Look," Idaho National Laboratory, Report INL/EXT-10-20722, January 2011.

27. S. Ploger, P. Demkowicz and J. Harp, "AGR-2 Irradiated Test Train Preliminary Inspection and Disassembly First Look," Idaho National Laboratory, Report INL/EXT-15-34997, May 2015.

28. S. A. Ploger, P. A. Demkowicz, J. D. Hunn and J. S. Kehn, "Ceramographic Examinations of Irradiated AGR-1 Fuel Compacts," Idaho National Laboratory, Report INL/EXT-12-25301, Rev. 1, September 2012.

29. B. Marsden and G. Hall, "Graphite in Gas-Cooled Reactors," in *Comprehensive Nuclear Materials*, Elsevier Ltd, 2012, pp. 325-390.

30. C. Folsom, C. Xing, C. Jensen, H. Ban and D. Marshall, "Experimental measurement and numerical modeling of the effective thermal conductivity of TRISO fuel compacts," *Journal of Nuclear Materials,* vol. 458, pp. 198-205, 2015.

31. IAEA, "Heat Transport and Afterheat Removal for Gas Cooled Reactors Under Accident Conditions," International Atomic Energy Agency, TECDOC-1163, 2000.

32. U. Littmark and J. F. Ziegler, Handbook of Range Distributions for Energetic Ions in All Elements, Pergamon Press, 1980.

33. A. H. Booth, "A Method of Calculating Fission Gas Release from UO_2 Fuel and Its Implication to the X-2-f Loop Test," Atomic Energy of Canada Limited, Report AECL 496, September 1957.

34. J. A. Turnbull and C. A. Friskney, "The Diffusion Coefficient of Gaseous and Volatile Species During the Irradiation of Uranium Dioxide," *Journal of Nuclear Materials,* vol. 107, pp. 168-184, 1982.

35. IAEA, "Fuel performance and fission product behaviour in gas cooled reactors," International Atomic Energy Agency, TECDOC-978, 1997.

36. IAEA, "IAEA, "Advances in High Temperature Gas Cooled Reactor Fuel Technology," International Atomic Energy Agency, TECDOC-1674, 2012.

37. D. Knoll and D. Keyes, "Jacobian-free Newton–Krylov methods: a survey of approaches and applications," *Journal of Computational Physics ,* vol. 193, pp. 357-397, 2004.

38. J. Hales, R. Williamson, S. Novascone, D. Perez, B. Spencer and G. Pastore, "Multidimensional multiphysics simulation of TRISO particle fuel," *Journal of Nuclear Materials,* vol. 443, pp. 531-543, 2013.

39. R. Price, "Properties of Silicon Carbide For Nuclear Fuel Particle Coatings," Nuclear Technology, vol. 35, no. 2, pp. 320-336, 1977.

40. Idaho National Laboratory, "Mechanistic Source Terms White Paper," Report INL/EXT-10-17997, July 2010.

41. D. Hewette, "High Temperature Fast Neutron Irradiation of Pyrolityc Carbon Coated ThO2 Microspheres," Carbon, vol. 7, no. 3, pp. 373-378, 1969.

42. Electric Power Research Institute, "Uranium Oxycarbide (UCO) Tristructural Isotropic (TRISO) Coated Particle Fuel Performance: Topical Report EPRI-AR-1(NP)," Report 30020199780, Palo Alto, CA, November 2020.

43. I.v. Rooyen, M. Dunzik-Gougar and P. v. Rooyen, "Silver (Ag) transport mechanisms in TRISO coated particles: A critical review," Nuclear Engineering and Design, vol. 271, pp. 180-188, 2014.

44. B.P. Collin, "AGR-1 Irradiation Test Final As-Run Report," Idaho National Laboratory," Report INL/EXT-10-18097, Rev. 3, January 2015.

45. B. P. Collin, "AGR-5/6/7 Irradiation Experiment Test Plan," Idaho National Laboratory, Report PLN-5245 Rev. 1, January 2018.

46. S. Wilks, "Determination of Sample Sizes for Setting Tolerance Limits," *Annals of Mathematical Statistics,* vol. 12, no. 1, pp. 91-96, 1941.

47. W. F. Skerjanc, J. T. Maki, B. P. Collin and D. A. Petti, "Evaluation of design parameters for TRISO-coated fuel particles to establish manufacturing critical limits using PARFUME," *Journal of Nuclear Materials,* vol. 469, pp. 99-105, 2016.

48. W. F. Skerjanc and B. P. Collin, "Assessment of Material Properties for TRISO Fuel Particles used in PARFUME," Idaho National Laboratory, Report INL/EXT-18-44631, August 2018.

49. P. A. Demkowicz, B.P. Collin, S. Ueta, and Y.M. Kim, " Generation IV Benchmarking of TRISO Fuel Performance Models Under Accident Conditions Final Report," Idaho National Laboratory for the Generation IV International Forum, Report INL/EXT-20-60147, October 2020.

Table 2-1. Primary Functions of Fuel Components

Layer	Purpose
UCO Kernel $UO_2 + UC + UC_2$	Contains fissile material Limits free oxygen release compared to traditional UO_2 $\Rightarrow$ suppresses CO production and subsequent kernel migration, over-pressure, and corrosion of SiC $\Rightarrow$ oxygen used to form less-mobile-than-carbides fission product oxides which reduces chemical attack of SiC
Porous Carbon Buffer	Provides void volume to accommodate fission gases and limit pressure buildup Mechanically decouples kernel from outer coating layers by accommodating swelling of UCO kernel Protects IPyC from fission products recoil
IPyC	Protects kernel during SiC deposition (chlorine attack) Protects SiC from fission product attack Secondary structural layer that puts SiC in compression and reduces risk of failure Fission gas barrier
SiC	Primary structural layer Primary fission product barrier
OPyC	Protects SiC layer during particle handling Secondary structural layer that puts SiC in compression and reduces risk of failure Fission gas barrier Provides bonding surface to overcoating matrix material
Overcoat	Prevents particle-to-particle contact during pebble fabrication Bonds to OPyC and allows pressing of coated particles into fuel annulus
Inner Core	Lowers overall density of the pebble and allows buoyancy in Flibe coolant
Fuel Annulus	Contains TRISO fuel particles Limits peak fuel temperature by placing TRISO particles closer to Flibe coolant, which allows higher particle power
Outer Shell	Protects TRISO fuel particles from potential mechanical or chemical damage and during fuel handling

Table 2-2. AGR-5/6/7 TRISO Fuel Properties

Property	Specified Range for Mean Value
Kernel diameter (μm)	425 ± 10
Buffer thickness (μm)	100 ± 15
PyC thickness (μm)	40 ± 4
SiC thickness (μm)	35 ± 3
Kernel density (g/cm^3)	≥ 10.4
Buffer density (g/cm^3)	1.05 ± 0.10
PyC density (g/cm^3)	1.90 ± 0.05
SiC density (g/cm^3)	≥ 3.19
C/U atomic ratio	0.40 ± 0.10
O/U atomic ratio	1.50 ± 0.20
PyC BAF	≤ 1.045 (IPyC) < 1.035 (OPyC)
SiC aspect ratio[a]	≤ 1.14

(a) Critical limit (mean value not specified)

Table 2-3. AGR-5/6/7 Specifications for Contamination and Defect Fractions

Property	Specified Fraction
Dispersed uranium fraction	$\leq 1.0 \times 10^{-5}$
Exposed kernel fraction	$\leq 5.0 \times 10^{-5}$
Defective SiC coating fraction	$\leq 1.0 \times 10^{-4}$
Defective IPyC fraction	$\leq 1.0 \times 10^{-4}$
Defective OPyC fraction	$\leq 1.0 \times 10^{-2}$

Table 2-4. KP-FHR Representative Pebble Dimensions and Properties

Property	Specified Mean Value
Inner core radius (mm) Fuel annulus inner radius (mm)	1.45
Fuel annulus outer radius (mm) Outer shell inner radius (mm)	1.85
Outer shell outer radius (mm)	2.0
Inner core density (g/cm^3)	1.23
TRISO particle density (g/cm^3)	3.0
TRISO particles packing fraction (%)	37

Fuel annulus density (g/cm^3)
     without TRISO particles
     with TRISO particles
	
	 1.75
	 2.21

Outer shell density (g/cm^3)	1.75

Table 2-5. Comparison of AGR Programs (UCO Fuel Only)

Irradiation Campaign Completion	AGR-1 (2009) AGR-2 (2013)	AGR-5/6(2020)	AGR-7 (2020)
Particles per Fuel Element	4,100 / 3,200	2,200 / 3,400	2,200
Packing Fraction	0.37	0.25 / 0.38	0.25
Particle Peak Power (mW)	100/150	190[a] / 140[a]	190[a]
Particle Average Power (mW)	60 / 70	130 / 80	100
U-235 Enrichment (at%)	19.5 / 13.8	15.3	15.3
Burnup (%FIMA)	19.6 / 13.2	13.2 / 10.0	12.9
Peak Fluence ($\times 10^{25}$n/m^2, E> 0.1 MeV)	4.8 / 3.9	4.8 / 3.9	4.9
Time (EFPD)	620 / 559	361	361

(a) Projected values

Table 2-6. KP-FHR Expected Normal Operating Conditions

[[

]]

Table 2-7. Irradiation Behavior of TRISO Fuel Particle Components

Coating Layer	Irradiation Behavior	Observation
Kernel	Swells outward	Pushes buffer outward
Buffer	Shrinks inward	Pulls IPyC inward if not debonded
IPyC / OPyC	Shrink early during irradiation and then start swelling later in irradiations as fast neutron fluence accumulates. Dimensional changes are anisotropic	Swelling starts radially at moderate fast neutron fluence levels and tangentially at higher fast neutron fluence levels
SiC	Elastic behavior	PyC shrinkage provides compressive stress Fission gas pressure causes tensile stress

Table 2-8. TRISO Fuel Failure Mechanisms Modeled in the Fuel Performance Analysis Model

[[

]]

Table 2-9. TRISO Fuel Failure Mechanisms Not Modeled in the Fuel Performance Analysis Model

[[

]]

Table 2-10. Phenomena Importance During Normal Operation and AOOs

[[

]]

Table 2-10. Phenomena Importance During Normal Operation and AOOs (continued)

[[

]]

Table 2-10. Phenomena Importance During Normal Operation and AOOs (continued)

[[

]]

Table 2-10. Phenomena Importance During Normal Operation and AOOs (continued)

[[

]]

Table 2-10. Phenomena Importance During Normal Operation and AOOs (continued)

[[

]]

Table 2-10. Phenomena Importance During Normal Operation and AOOs (continued)

[[

]]

Table 2-10. Phenomena Importance During Normal Operation and AOOs (continued)

[[

]]

Table 2-11. Phenomena of Importance During Postulated Accidents

[[

]]

Table 3-1. Polynomial Coefficients for PyC Irradiation-induced Dimensional Changes

[[

]]

[[

]]

Table 3-2. Pyrocarbon Isotropic Strain as a Function of Density

[[

]]

Table 3-3. Difference between PyC Radial and Tangential Strains as a Function of Density

[[

]]

Table 3-4. PyC Anisotropy (BAF) as a Function of Fast Neutron Fluence

[[

]]

Table 3-5. Young's Modulus for SiC

[[

]]

Table 3-6. Coefficients for Unirradiated Fuel Matrix Thermal Conductivity

[[

]]

Table 3-7. Decay Constants for the Short-lived Kr and Xe Isotopes

Isotope	Decay constant λ (s^{-1})
^{85m}Kr	4.298×10^{-5}
^{87}Kr	1.520×10^{-4}
^{88}Kr	6.780×10^{-5}
^{89}Kr	3.656×10^{-3}
^{90}Kr	2.146×10^{-2}

Isotope	Decay constant λ (s^{-1})
^{131m}Xe	6.730×10^{-7}
^{133}Xe	1.528×10^{-6}
^{135}Xe	2.116×10^{-5}
^{135m}Xe	7.551×10^{-4}
^{137}Xe	3.008×10^{-3}
^{138}Xe	8.193×10^{-4}
^{139}Xe	1.733×10^{-2}

Table 3-8. Diffusion coefficients for Key Fission Products Modeled in KP-BISON

	D_1 (m^2/s)	Q_1 (kJ/mol)	D_2 (m^2/s)	Q_2 (kJ/mol)
Cesium				
Kernel	5.6×10^{-8}	209	5.2×10^{-4}	362
Buffer & Buffer-IPyC Gap	10^{-8}	0	-	-
PyC	6.3×10^{-8}	222	-	-
SiC	$5.5\times10^{-14}\times e^{1.1\times\phi/5}$ ϕ is the fast neutron fluence (x10^{25} n/m^2, E_n > 0.18 MeV)	125	1.6×10^{-2}	514
Matrix	3.6×10^{-4}	189	-	-
Strontium				
Kernel	2.2×10^{-3}	488	-	-
Buffer & Buffer-IPyC Gap	10^{-8}	0	-	-
PyC	2.3×10^{-6}	197	-	-
SiC	1.2×10^{-9}	205	1.8×10^6	791
Matrix	1.0×10^{-2}	303	-	-
Silver				
Kernel	6.7×10^{-9}	165	-	-
Buffer & Buffer-IPyC Gap	10^{-8}	0	-	-
PyC	5.3×10^{-9}	154	-	-
SiC	3.6×10^{-9}	215	-	-
Matrix	1.6	258	-	-
Krypton (Iodine, Xe)				
Kernel - Normal Operation	1.3×10^{-12}	126	-	-
Kernel - Accident	8.8×10^{-15}	54	6.0×10^{-1}	480
Buffer & Buffer-IPyC Gap	10^{-8}	0	-	-
PyC	2.9×10^{-8}	291	2.0×10^5	923
SiC - T>1625.9 K	3.7×10^1	657	-	-
SiC - T≤1625.9 K	8.6×10^{-10}	326	-	-
Matrix	6.0×10^{-6}	0	-	-

Table 3-9. KP-BISON Material Properties

Fuel component	Description
Kernel	
Swelling	Volumetric expansion resulting from fissioning
Elastic modulus	Determines elastic behavior
Poisson's ratio	
Thermal conductivity	Dictates fuel temperature
Specific heat capacity	Dictates fuel temperature during transients
Buffer	
Elastic modulus	Determines elastic behavior
Poisson's ratio	
Irradiation-induced creep	Relieves stress caused by shrinkage
Poisson's ratio in creep	
Irradiation-induced dimensional change	Puts layer under stress potentially leading to its fracture
Thermal conductivity	Dictates fuel temperature
Specific heat capacity	Dictates fuel temperature during transients
Thermal expansion	Volumetric expansion resulting from temperature
Weibull parameters	Determines statistical failure
PyC	
Elastic moduli	Determines elastic behavior
Poisson's ratio	
Irradiation-induced creep	Relieves stress caused by shrinkage
Poisson's ratio in creep	
Irradiation-induced dimensional change	Puts layer under stress potentially leading to its cracking
Thermal conductivity	Dictates fuel temperature
Specific heat capacity	Dictates fuel temperature during transients
Thermal expansion	Volumetric expansion resulting from temperature
Weibull parameters	Determines statistical failure
Buffer-IPyC interface	
Heat transfer across buffer-IPyC gap	Dictates fuel temperature
SiC	
Elastic modulus	Determines elastic behavior
Poisson's ratio	
Thermal conductivity	Dictates fuel temperature
Specific heat capacity	Dictates fuel temperature during transients
Thermal expansion	Volumetric expansion resulting from temperature
Weibull parameters	Determines statistical failure

Table 3-9. KP-BISON Material Properties (continued)

Fuel Component	Description
Matrix	
Thermal conductivity	Dictates fuel temperature
Specific heat capacity	Dictates fuel temperature during transients
Kernel, coating layers, and matrix	
Diffusion coefficients of fission products	Release of fission products to the coolant

Table 3-10. KP-BISON Physical Models

Physical model	Description
Strain-displacement and stress-strain constitutive relationship	Mechanical state of the particle and stresses, strains, and displacements in the kernel and coating layers
Failure fraction	Determination of probability of failure of coating layers
Heat equation	Thermal state of the particle and temperature profile across the kernel and coating layers
Fission yields	Generation of fission products
Fission gas release	Generation of internal pressure
Internal fission gas pressure	Stress state of the particle potentially leading to its failure
Pd penetration	Corrosion of the SiC layer potentially leading to its failure
R/B	Indicator of full TRISO failure
Fission product transport (Fickian diffusion)	Release of fission products to the coolant

Table 4-1. Fuel Property Parameters for Uncertainty Analysis

[[

]]

Table 4-2. Material Properties Considered in Uncertainty Analysis

Property	Input Parameters
Kernel	
Swelling	Burnup[a,b]
Elastic modulus	Theoretical density[b] Density Temperature
Poisson's ratio	Theoretical density[b] Density
Thermal conductivity	Temperature
Specific heat capacity	Molar mass[b] Temperature
Buffer	
Elastic modulus	Density Fast fluence Temperature
Poisson's ratio	Constant
Irradiation-induced creep	Density Temperature
Poisson's ratio in creep (constant)	none
Irradiation-induced dimensional change	Density Fast fluence Temperature
Thermal conductivity	Density
Specific heat capacity (constant)	none
Thermal expansion	Temperature
PyC	
Elastic moduli	Density Initial BAF Fast Fluence Temperature
Poisson's ratio (constant)	none
Irradiation-induced creep	Density Temperature
Poisson's ratio in creep (constant)	none

Irradiation-induced dimensional change	Density
	BAF
	Fast fluence
	Temperature
Thermal conductivity (constant)	none
Specific heat capacity (constant)	none
Thermal expansion	BAF
	Temperature
Characteristic strength	Fast fluence
	Temperature
Weibull modulus (constant)	none
Buffer-IPyC gap	
Heat transfer	Kr/Xe molar fractions
	Temperature
SiC	
Elastic modulus	Temperature
Poisson's ratio (constant)	none
Thermal conductivity	Temperature
Specific heat capacity	Temperature
Thermal expansion (constant)	none
Characteristic strength (constant)	none
Weibull modulus (constant)	none
Matrix	
Thermal conductivity	Density
	Fast fluence
	Temperature
	Packing fraction
Specific heat capacity	Density
	Temperature

(a)   Depends on the density and fission rate.
(b)   Depends on the [235]U enrichment and C/U and O/U ratios.

Table 4-3. Physical Models Considered in Uncertainty Analysis

Model	Input Parameters
Failure fraction	Tangential stress Characteristic strength Weibull modulus
Heat equation	Density Temperature Thermal conductivity Specific heat capacity Fission rate
Fission yields	Burnup
Fission gas release (long-lived isotopes)	Kr/Xe fission yields Kr/Xe molar fractions Kernel radius Kernel density C/U and O/U ratios Grain size Temperature
Internal fission gas pressure	Kr/Xe moles Void volume[a] Temperature
Pd penetration	Temperature
Release rate to birth rate ratio (short-lived isotopes)	Temperature
Fission product transport	Fission Rate Fission Yields Diffusion Coefficients Temperature

(a) Calculated from initial porosities of kernel and buffer and irradiation-induced dimensional changes of kernel (swelling) and buffer and IPyC layers (shrinkage/swelling).

Table 4-4. Irradiation Conditions Considered in Uncertainty Analysis

Neutronic (ν) or T/H Codes	Related KP-BISON Input	TRISO Models
Fission rate density	Fission rate density	Burnup[a]
Fast neutron flux	Fast neutron flux	Fast neutron fluence[b]
Pebble surface temperature [c]	Pebble surface temperature	Pebble surface temperature
Irradiation length	Irradiation time steps	Time

(a) Burnup depends on kernel density and fission rate density.
(b) Fluence is the accumulated flux, i.e., the integral of flux over time.
(c) Obtained by a heat transfer calculation between the pebble and surrounding coolant.

Table 6-1. Contributors to Fission Product Release

[[

]]

Table 6-2. Limits of KP-BISON Code Applicability

[[

]]

Figure 2-1. Graphical Description of a TRISO-coated Particle
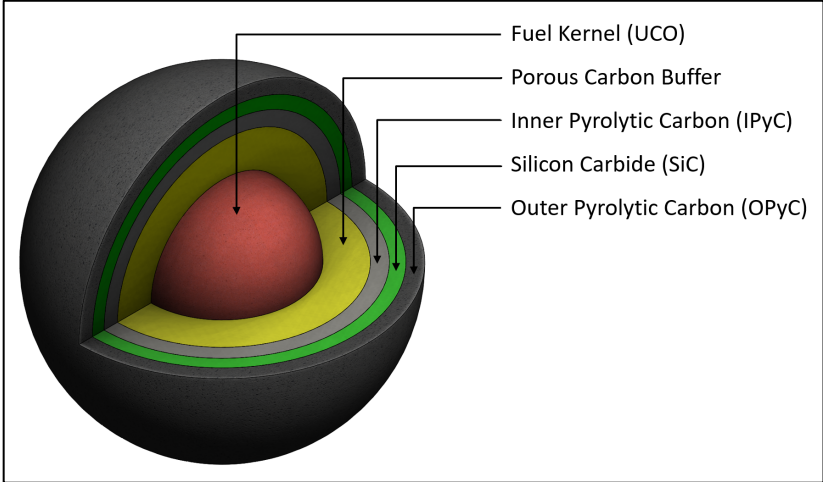
Fuel Kernel (UCO)

Porous Carbon Buffer

Inner Pyrolytic Carbon (IPyC)

Silicon Carbide (SiC)

Outer Pyrolytic Carbon (OPyC)

Figure 2-2. Notional Design of the TRISO Particles Embedded in a Spherical Pebble
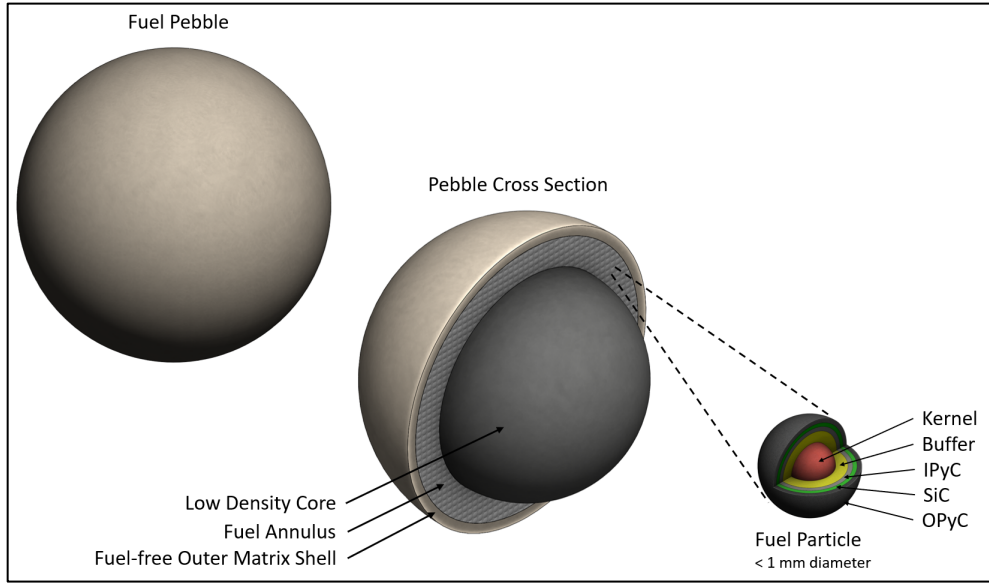
Figure 2-3. Behavior of Coating Layers in TRISO Fuel Particle
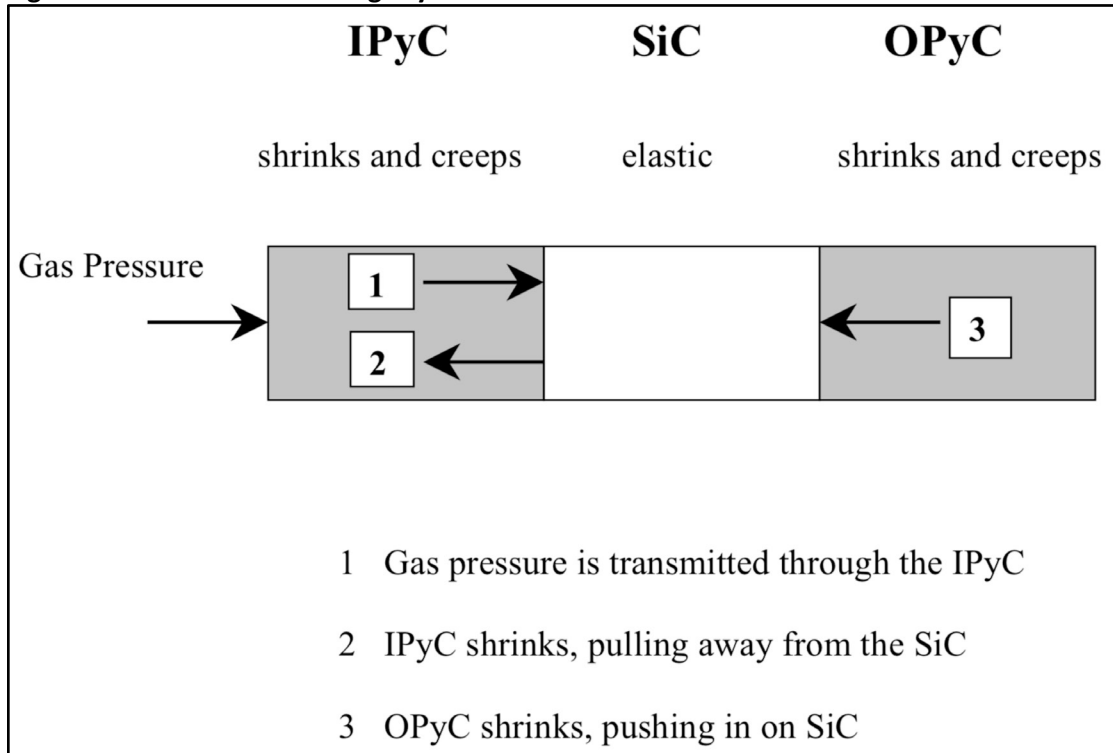
Source: G. K. Miller et al., "Consideration of the effects on fuel particle behavior from shrinkage cracks in the inner pyrocarbon layer," Figure 2 of Reference 6.

Figure 2-4. Representative Stress Histories of the IPyC and SiC Layers for an Intact UCO TRISO Particle (Illustration Only)
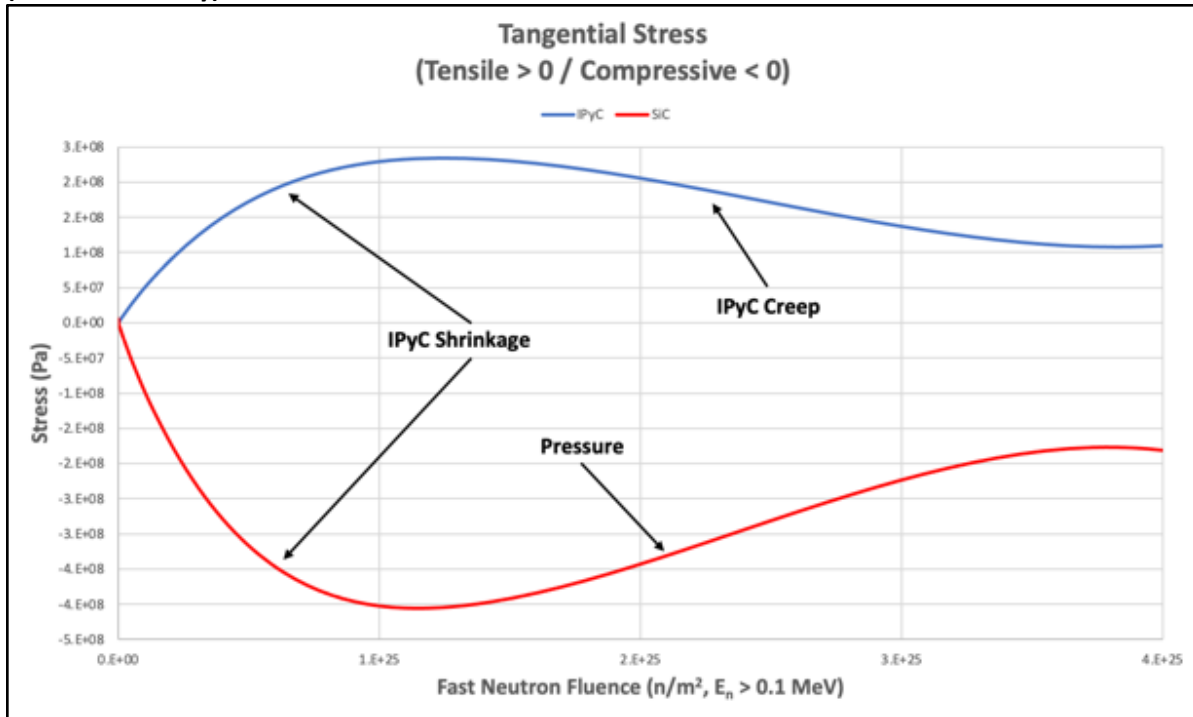
Figure 2-5. Fission Product Release
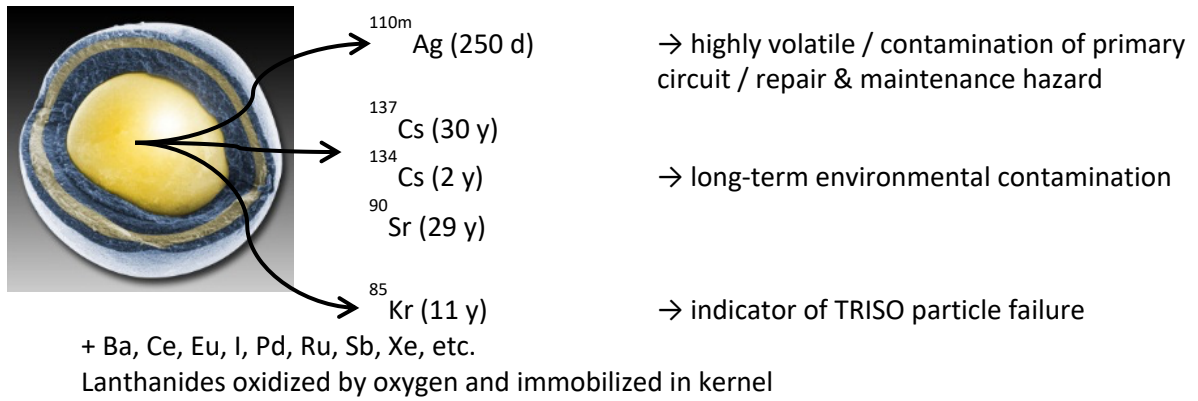
^{110m}Ag (250 d) → highly volatile / contamination of primary circuit / repair & maintenance hazard

^{137}Cs (30 y)

^{134}Cs (2 y) → long-term environmental contamination

^{90}Sr (29 y)

^{85}Kr (11 y) → indicator of TRISO particle failure

+ Ba, Ce, Eu, I, Pd, Ru, Sb, Xe, etc.

Lanthanides oxidized by oxygen and immobilized in kernel

[[

Figure 4-1. Fuel Property Sampling

]]

Figure 4-2. Distributions of Kernel Diameter for AGR Fuel

[[

]]

Figure 4-3.Range of Variation of Kernel Diameter

[[

]]

Figure 4-4. Sampling of Allowable Range of Variation for Average Value of Fuel Property

[[

]]

Figure 4-5. Inner Loop Calculation Scheme for Failure Probability

[[

]]

Figure 4-6. Inner Loop Calculation Scheme for Fission Product Release Fraction

[[

]]

Figure 4-7. Flow chart of Uncertainty Determination Process\

[[

]]

Figure 6-1. KP-BISON Calculation Flow Chart

[[

]]

Figure 6-2. KP-BISON Scheme for Failure Fraction of TRISO Particles

[[

]]

Figure 6-3. Example Finite Element Model for a TRISO particle having a Radial IPyC Crack
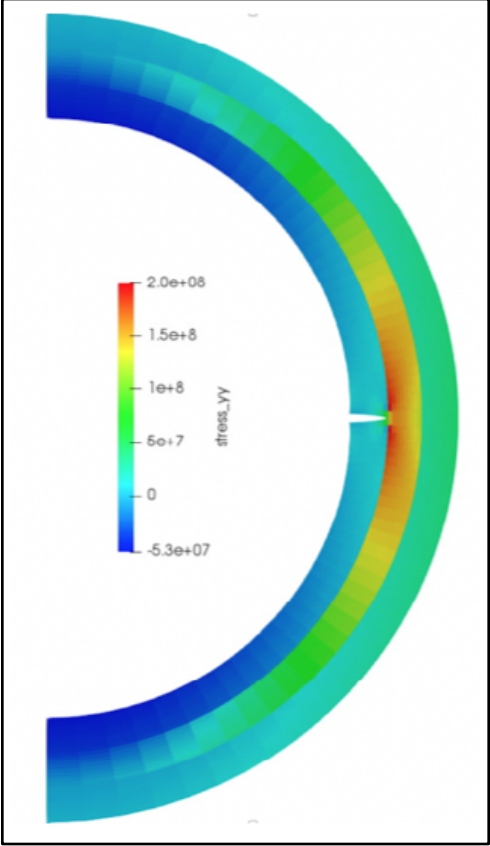
Figure 6-4. Example Tangential Stress for Spherical and Aspherical TRISO Particles
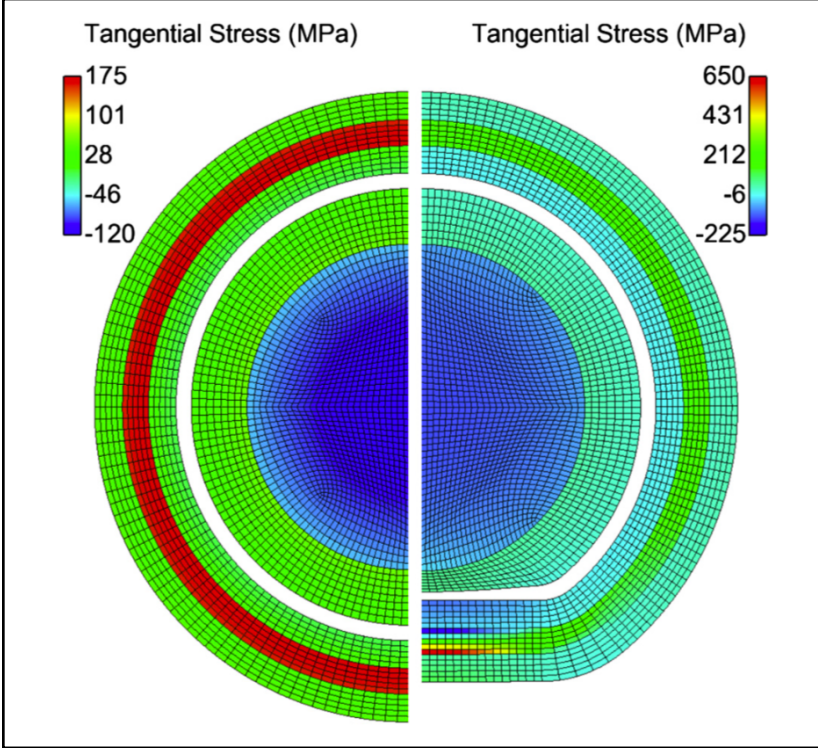
Figure 6-5. KP-BISON Scheme for Fission Product Release from TRISO Particles

[[

]]

Figure 6-6. Design Interfaces for Fuel Performance Calculation
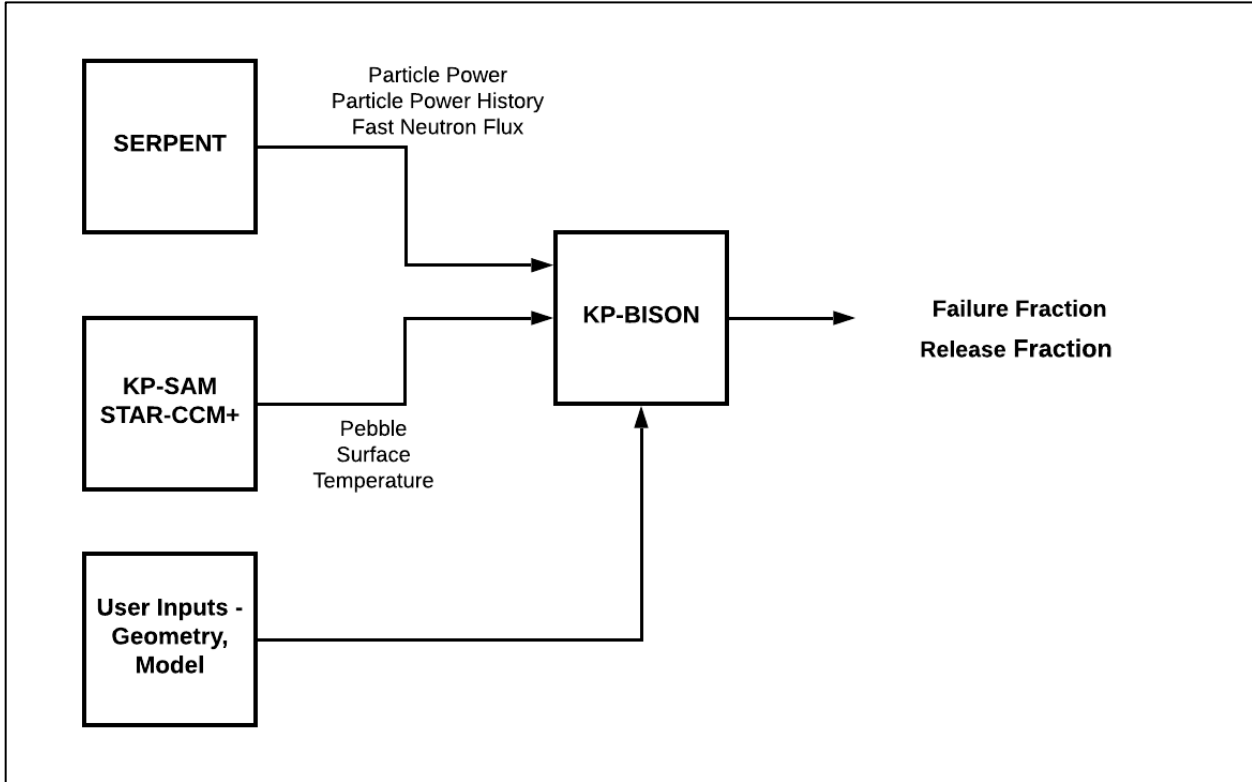
APPENDIX A.   CONVERSION FACTORS FOR FUEL UTILIZATION

Fuel utilization is usually defined using GWd/t in nuclear reactor core studies and %FIMA in fuel studies. For conversion purposes, it is assumed that the binding energy released by the fission of an atomic nucleus in a ^{235}U fuel system is 200 MeV on average. The following chain of conversion ensues:

1 fission = 200 MeV = 3.20×10^{-11} J = 3.71×10^{-25} GWd

At enrichments lower than 20 wt% ^{235}U, the atomic mass of the initial heavy metal content of the kernel (mainly ^{235}U and ^{238}U) is ~238 g/mol. Hence, using Avogadro's number (6.022×10^{23} at/mol), each initial metric ton of fissile material contains ~2.53×10^{27} atoms. This results in the following conversion factors:

1% FIMA = 9.4 GWd/t
1 GWd/t = 0.11% FIMA

APPENDIX B. ELASTIC PROPERTIES OF THE KERNEL

[[

]]

Figure B2. Temperature Dependence of Young's Modulus of UO₂

[[

]]

Table B1. Relative Difference Between Digitized Data and Temperature Dependent Fits

[[

]]

[[

]]

APPENDIX C.   KP-BISON EXAMPLE RESULTS

KP-BISON was used to perform preliminary calculations and provide example results showing its capabilities. The results in this appendix were obtained from an unvalidated and unverified version of KP-BISON. Furthermore, the study cases are based on irradiation conditions that are representative but not precisely the irradiation conditions expected in KP-FHR cores.

C.1 Design and Assumptions

Table C1 shows approximate values that are expected to bound the performance parameters of the various configurations of the KP-FHR core. The "baseline" parameters were used for a study on mesh optimization and convergence.

Table C1. Example TRISO Fuel Performance Parameters in KP-FHR Cores.

[[

]]

[[

]]

[[

]]

Mesh convergence

[[

]]

[[

]]

[[

]]

[[

]]

[[

]]

[[

]]

C.2 KP-FHR Example Results

The results for the startup, transition, and equilibrium KP-FHR core configurations are presented below.

[[

]]

[[

]]

[[

]]

[[

]]

[[

]]

[[

]]

[[

]]

[[

]]

[[

]]

[[

]]

[[

]]

APPENDIX D.   KP-BISON UNCERTAINTY QUANTIFICATION SAMPLE RESULTS

[[

]]

[[

]]

[[

                                                                        ]]

[[

]]

[[

]]

[[

]]